DEVELOPMENT OF ULTRA- FINE GRAINED ALUMINIUM BY SEVERE PLASTIC DEFORMATION

A Thesis
Submitted in partial fulfillment of the requirements for the award of the Degree of

MASTER OF TECHNOLOGY

in

NEW MATERIALS AND PROCESSING TECHNOLOGY

BY

WAHDAT ULLAH

(M.TECH /NMPT/07/05)

DEPARTMENT OF APPLIED PHYSICS
BIRLA INSTITUTE OF TECHNOLOGY
MESRA-835215, RANCHI
2006

DECLARATION CERTIFICATE

This is to certify that the work presented in this thesis entitled **"DEVELOPMENT OF ULTRA-FINE GRAINED ALUMINIUM BY SEVERE PLASTIC DEFORMATION"** in partial fulfillment of the requirement for the award of degree of **Master of Technology in New Materials and Processing Technology** of Birla Institute of Technology, Mesra, Ranchi is an authentic work carried out at the National Metallurgical Laboratory (Jamshedpur) under our joint supervision and guidance.

To the best of our knowledge, the content of this thesis does not form a basis for the award of any previous degree to any one else.

Dr. P. K. Barhai
Professor
Birla Institute of Technology
Ranchi-835215

Dr. V. C. Srivastava
Scientist
National Metallurgical Laboratory
Jamshedpur-831007

Head
Department of Applied Physics
Birla Istitute of Technology
Mesra,Ranchi-835215

Dean
(Post Graduate Studies)
Birla Institute of Technology
Mesra,Ranchi-835215

CERTIFICATE OF APPROVAL

The foregoing thesis entitled "**DEVELOPMENT OF ULTRA FINE GRAINED ALUMINIUM BY SEVERE PLASTIC DEFORMATION**" is hereby approved as a creditable study of research topic and has been presented in a satisfactory manner to warrant its acceptance as prerequisite to the degree for which it has been submitted.

It is understood that by this approval, the undersigned do not necessarily endorse any conclusion drawn or opinion expressed therein, but approve the thesis for the purpose for which it is submitted.

(Internal Examiner) **(External Examiner)**

Head of the Department
(Chairman)

CONTENTS

ACKNOWLEDGEMENTS

I would like to express my deep sense of gratitude to Dr. V. C. Srivastava, Scientist, Metal Extraction and forming Division, National Metallurgical Laboratory (NML), Jamshedpur, and Dr. P. K. Barhai, Dean, Sponsored Research & Collaborative projects and Professor & Head, Department of Applied Physics, B.I.T. Mesra, Ranchi for their invaluable suggestions, excellent supervision, constant encouragement and critical discussion throughout the research work and during the preparation of the manuscript. The inspiration and friendly attitude of Dr. V. C. Srivastava at every stage of this work is duly appreciated. It is indeed a great pleasure to be associated with him.

I am grateful to Professor S. P. Mehrotra, Director, National Metallurgical Laboratory, Jamshedpur, for allowing me to carry out the project work and permitting the use of necessary facilities for successful completion of the work.

My sincere thanks to Dr. Sandip Ghosh Chowdhury, Dr. Mainak Ghosh, Dr. A. K. Parmanik, Dr. Venkateswarlu for their selfless support in texture and microstructural analysis and also for their constant encouragement and fruitful suggestions. I would also thank Dr. Goutam Das, for extending necessary facilities for optical microscopy.

I take this opportunity to thank Mr. P. K. De and Mr. A. Srinivasan, Scientists, MEF Division, NML, Jamshedpur, for their constant encouragement, inspiration, assistance and useful discussion throughout the project work. I would also like to thank Mr. B. A. Lakra and Mr. M. Gunjan for their kind support in hardness measurement and scanning electron microscopy of materials.

I express my deep sense of gratitude to Dr. G. G. Sarkar, Principal Scientific officer, and Dr. S. K. Sinha, Reader, Department of Applied Physics, B.I.T. Mesra, Ranchi, for their kind support and advice rendered during the course of my project work.

I also thank Dr..K. L. Hansda, Scientist (NML) for his constant encouragement and support throughout my stay at NML, Jamshedpur.

I also take this opportunity to extend my thanks and gratitude towards all the members of the faculty of Applied Physics Department, B.I.T. Mesra, Ranchi, for their help in connection with this project work.

I would also like to thank my friends and fellow colleagues Mr. Ravi Shekhar, Mr. Randhir kumar, Mr. Sunil Tewary, Mr. Parshant Srivastava and many others who have assisted me at all moments of need. Thanks to all other members of the faculty of B.I.T. Mesra, and NML, Jamshedpur for their help, yet uncounted in making this project and to see the light of success. Finally, I thank all personalities who either directly or indirectly rendered help to complete the project work successfully.

I express my profound gratitude to my parents for their sacrifices, constant support, understanding and encouragement extended.

Date: 28.05.2007 Wahdat Ullah
Place: Ranchi M.Tech.(B.I.T,Mesra)

PREFACE

Nanoscale science and technology is experiencing a rapid development and nano-materials have made profound impact on every field of materials research. Scientists believe that the nanoscale science and technology will bring revolutions in human history due to the unique properties of nano-materials. Nanomaterials are the fundamental basis of nanotechnology. Two basic and complementary approaches have been developed for the synthesis of nanomaterials. These are known as “bottom up” and “top down” approaches. In the bottam up approach, atoms, molecules and even nanosize particles themselves can be used as the building blocks for the creation of complex nanostructures. Whereas, in the “tops down” approach coarse-grained materials are refined into ultrafine -grained /nanostructured materials. Ultrafine grained (UFG) materials may be defined as polycrystalline materials having average grain size less than ~1μm. The grain sizes of UFG materials may lie within the sub-micrometer (100-1000 nm) range.

In order to convert a coarse grained solid into a material with ultrafine grains, it is necessary to impose an exceptionally high strain in order to introduce a high density of dislocations which, in turn, re-arrange to form an array of grain boundaries with increase in strain. Conventional metal forming procedures, such as extrusion or rolling, are restricted in their ability to produce UFG structures for two important reasons. First, there is a limitation on the overall strains that may be imposed using these procedures because a very high strain requires corresponding reductions in the cross-sectional dimension of the work-pieces. Second, the strains imposed in conventional processing are limited and insufficient to give rise to UFG structures because of the generally low workability of metallic alloys at ambient temperatures. Another conventional method, such as rapid solidification and vapor condensation, are able to refine the materials up to nanoscale, but these processes are restricted to only thin layers/sections. As a consequence of these limitations, there is a paradigm shift in the synthesis routes for nanoscale materials and alternative processing techniques have evolved. The severe plastic deformation (SPD) technique is one of such processes, where extremely high strains are imposed at relatively low temperatures.

During the last two decade SPD has emerged as a widely known procedure for the grain refinement of metals and alloys into sub-micrometer or even nanometer range. Synthesis of UFG materials by SPD refers to various experimental procedures of metal forming that may be used to impose very high strains on materials leading to exceptional grain refinement. For production of bulk UFG materials with equiaxed microstructure and high angle grain boundary misorientation, accumulative roll bonding (ARB) and equal channel angular pressing are the two well known SPD methods.

Materials processed by SPD have shown superior mechanical properties such as high strength, excellent fatigue life, high toughness and low temperature superplasticity. As the specific material properties are becoming stringent in the current developmental scenario, there is a continuing increase in market requirements for high-strength metals and alloys. This finds applications in aerospace, automobile, transportation, food and chemical processing, electronics, and conventional defence industries. The market emphasis and exceptional material properties requirements have led to a considerable interest in the development of ultrafine-grained/nanomaterials by severe plastic deformation.

Therefore, the present work has been undertaken to develop ultrafine-grained aluminum by severe plastic deformation method and to examine the microstructure and mechanical properties by different characterizing tools. An important objective of this work is to identify and quantify interrelationships between the deformation mechanisms active during grain refinement process and to determine their influence on the mechanical behavior of UFG aluminum processed by accumulative roll bonding technique, one of the variants of severe plastic deformation.

CHAPTER - I

Literature Review

1. LITERATURE REVIEW

1.1 Modern trends of ultrafine-grained materials forming

As has been already mentioned in the previous section, there are two different approaches for the synthesis of UFG (Zhu and Liao, 2004), in the present section we attempt to illustrate these approaches in detail. A schematic representation of processing routes and their effect on final grain size refinement is given in figure 1.1. It is obvious from the figure that accumulative roll bonding (ARB) and ECAP, variants of severe plastic deformation, can be effectively used to produce UFG materials. Nanomaterials find numerous applications depending upon the structure and property variation obtained during processing. A summary of the possible variation in the specific properties of nanomaterials is shown in figure 1.2. This describes the variation when the material reaches in nanoscale regime. The synthesis route of nanomaterials can be divided into two broad approaches which are described in the following sections.

1.1.1 Bottom up approach

In the "bottom-up" approach of synthesis, atoms, molecules and even nanoparticles can be used as the building blocks for the creation of complex structures. Most of the bottom-up approaches emphasize use of nanopowders for the synthesis of nanostructured materials. For structural applications, the nanopowders need to be consolidated into bulk nanostructured materials. Examples of these techniques include inert gas condensation (Gleiter, 1981 and 1989), electrodeposition (Erb et al.,1993), ball milling with subsequent consolidation (Koch and Cho, 1992) and cryomilling with hot isostatic pressing (Luton et al.,1989 and Witkin and Lavernia, 2006). In practice, these

techniques are often limited to the production of fairly small samples that may be useful for applications in fields such as electronic devices but are generally not appropriate for large-scale structural applications. Furthermore, the finished products from these techniques invariably contain some degree of residual porosity and a low level of contamination, which is introduced during the fabrication procedure. Recent research has shown that large bulk solids, in an essentially fully-dense state, may be produced by combining cryomilling and hot isostatic pressing with subsequent extrusion (Han et al., 2004) but the operation of this combined procedure is expensive and at present it is not easily adapted for the production and utilization of structural alloys in large-scale industrial applications.

1.1.2 Top-down approach

The "top-down" processes are effective examples of solid-state processing of materials. In this synthesis approach, coarse-grained materials are refined into nanostructured materials through heavy straining or shock loading. This approach obviates the limitation of small product sizes and also the contamination that is inherent features of materials produced using the ''bottom-up'' approach. This has an additional advantage that it can be readily applied to a wide range of pre-selected alloys. The first observations of the production of UFG microstructures using this approach appeared in the scientific literature in the early 1990s. (Valiev et al., 1990 and Valiev et al., 1991). It is important to note that these early publications provided a direct demonstration of the ability to employ heavy plastic straining in the production of bulk materials having fairly homogeneous and equiaxed microstructures with grain sizes in the submicrometer range.

1.2 Severe plastic deformation

Severe plastic deformation term (SPD) is a modified form of "intensive plastic deformation". The term severe plastic deformation was first introduced by Musalimove and Valiev in 1992, where they described the deformation of an Al-4% Cu-0.5%Zr alloy [R.S. Musalimove and R.Z. Valiev (1992)]. In the last decade, this process established

itself very well as an effective method for the production of bulk ultra fine-grained (UFG) metallic materials (Valiev et al., 1993; Valiev et al., 2000; Valiev, 2004). Several methods of SPD are now available for refining the microstructure in order to achieve superior strength and other properties e.g.

* Equal-channel angular pressing (ECAP) (Valiev et al., 1991, Segal et al., 1981)
* High-pressure torsion (HPT) (Smirnova et al., 1986; Zhilyaev et al., 2003)
* Multi-directional forging (Salishchev et al., 1993; Valitov et al., 1994; Sitdikov et al., 2004)
* Twist extrusion (Beygelzimer et al., 2004; Varyutkhin et al., 2006)
* Cyclic-extrusion/compression (Richert and Ritchert, 1986; Richert et al., 1999)
* Reciprocating extrusion (Chu et al., 2001)
* Repetitive corrugation and straightening (RCS) (Huang et al., 2001; Zhu et al., 2001)
* Constrained groove pressing (CGP) (Shin et al., 2002)
* Cylinder covered compression (CCC) (Zhao et al., 2004)
* Accumulative roll-bonding (ARB) (Saito et al., 1998)
* Friction stir processing (FSP) (Rhodes et al., 1997; Mishra and Ma, 2005)
* Submerged friction stir processing (SFSP) (Hofmann and Vecchio, 2005)

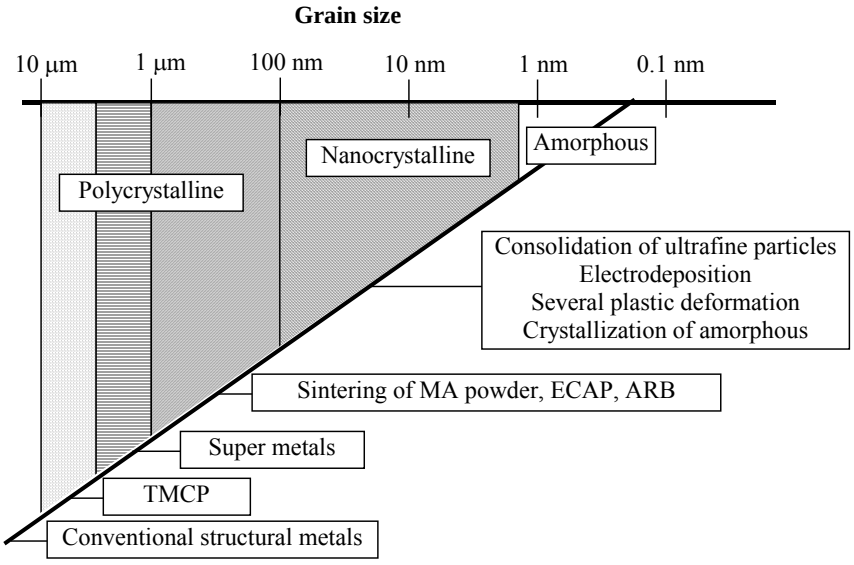

Fig. 1.1: Typical grain size range generated by different materials

All of these procedures are capable of introducing large plastic strain leading to significant microstructural refinement in bulk crystalline solids. Some of these techniques, such as ARB, ECAP, multi-directional forging and HPT, are already well-established methods for producing UFG materials where, depending upon the crystal structure, the processed microstructures have grain sizes lying typically within the range of ~70–500 nm. The other techniques are currently under development for this purpose. Of these various procedures, **accumulative roll bonding (ARB)** process of metal forming is an especially attractive processing technique for producing **ultrafine grained (UFG)** materials (Tsuji et al., 2003; Li et al., 2006; Lee et al., 2002). It is a simple procedure that makes use of a conventional roll bonding procedure, which is easily performed on a wide range of metals and alloys. Processing by ARB uses equipments that are readily available in most laboratories. These attractive features have led to many experimental studies and new developments in ARB processing over the last decade.

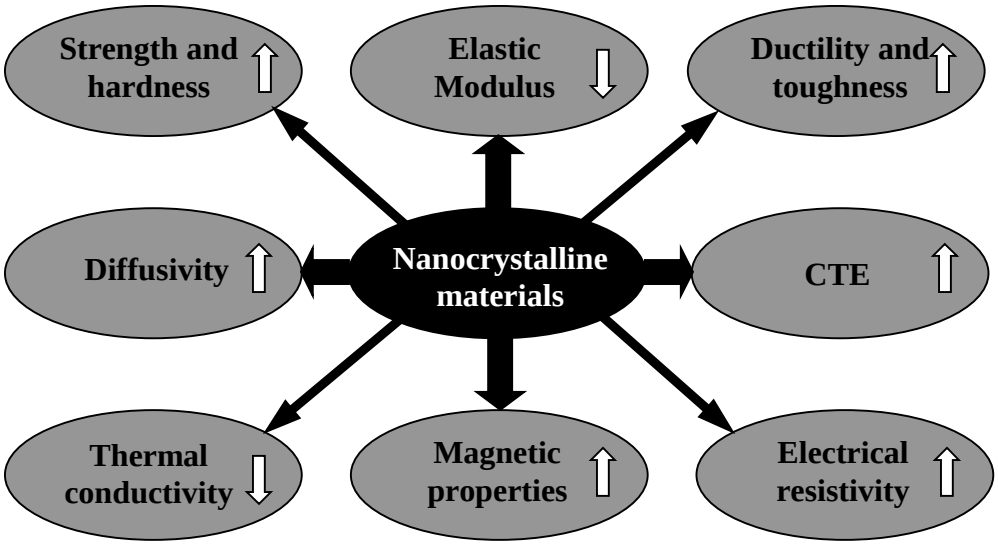

Fig. 1.2 : A summary of the properties of nanocrystalline materials

In view of the above-mentioned developments, the present work aims at developing ultrafine-grained commercial purity Aluminium. The proposed work involves processing of materials through SPD, examination of microstructural features and evaluation of mechanical properties of the product material. In the following sections, we

have attempted to give a brief introduction to accumulative roll bonding and equal channel angular pressing, most commonly used severe plastic deformation processes.

1.2.1 Accumulative Roll Bonding (ARB)

1.2.1.1 ARB Process

The ARB process, which forms the basis of this study, can be explained on the basis of a schematic diagram, as shown in Fig. 1.3. In this process, thin sheets of metal/alloy are taken and stacked together for roll bonding. The surfaces to be joined are roughened and cleaned; the two parts are stacked and roll bonded with approximately 50% reduction in thickness. The bonded sheet is cut into two halves and again stacked after proper surface cleaning and rolled. Several researchers have shown that the process may be repeated several times, if some precautions like removing the edge cracks are taken. Several passes of repeated roll bonding may lead to a large reduction in the initial sheet thickness. A little consideration would indicate that after six such passes a total number of 64 layers could be introduced. This means that an initial 2 mm thick sheet would be reduced to (2/64) mm if a reduction of 50% is achieved during each pass. This process can be carried out either in hot condition or cold condition. However, it is beneficial to work bellow the recrystallisation temperature of the materials. If $T_{homologous}$ of roll bonding is close to $0.5T_m$, sound bonding is achieved by reduction of approx. 50%. However, it may vary from materials to materials. Hence, the material can be bonded together without recrystallization. ARB can be used to introduce ultra high plastic strain without any geometrical change, if reduction is maintained to 50% in every rolling pass, as increase in width is negligible if the aspect ratio, i.e., ratio of width to thickness is >10. If reduction is 50% per cycle, the thickness of initial strip after n cycles is

$$t = \frac{t_0}{2^n}$$

where t_0 = initial thickness of strips.

Total reduction $r_t = \frac{t_0 - t}{t_0} = 1 - \frac{t}{t_0} = 1 - \frac{1}{2^n}$

The assumption of von Mises yield criterion (Krallics and Lenard, 2004) and plane strain condition, i.e., no lateral spreading, the equivalent plastic strain is

$$\varepsilon = \left(\frac{2}{\sqrt{3}}\right) \ln\left(\frac{t_{initial}}{t_{final}}\right)^n$$

$$= 0.80 \text{ n}$$

$$= 4.80 \text{ (for 6 passes)}$$

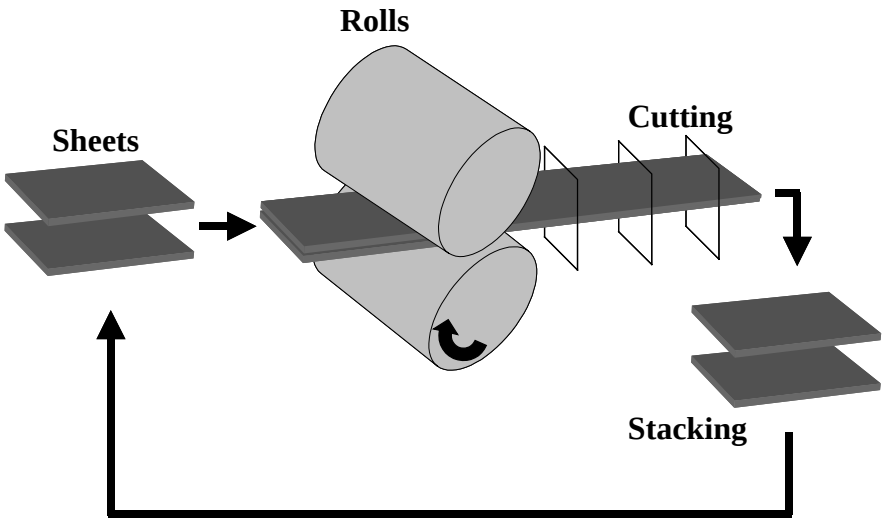

Fig. 1.3: Schematic diagram showing ARB process

There are two possible additional mechanisms in the ARB process, which differ from other high straining processes. The first possible mechanism is the effect of severe shear deformation just below the surface. It has been reported that severe shear deformation is introduced by friction between the work piece and the roll under dry conditions. This shear deformation significantly increases the equivalent strain and promotes grain refinement (Li et al., 2006). Moreover, these highly deformed surface layers are further introduced into the interior of the material by repetitive folding and

rolling. The other mechanism is the introduction of new interfaces. A large number of interfaces are introduced by several ARB cycles. These interfaces show a well-developed fibrous structure. The oxide films on the surfaces, as well as inclusions, are dispersed uniformly by repetition. These second phase particles contribute to strengthening and may act as obstacle for grain growth (Lee et al., 2002).

1.2.1.2 Phenomena affecting interfacial bonding

It is obvious from previous sections that accumulative roll bonding process is a cold welding process forming a bond between participating metallic layers. The strength of bonds depends on several metallurgical and mechanical factors. And also, the bond quality reflects its presence in the mechanical properties of the ARBed materials. Therefore, a good bonding between layers becomes of paramount importance in this process. The bond quality, in general, depends on the following material and process parameters. (Krallics and Lenard, 200).

- The grain size and ductility of the materials
- Cleanliness and roughness of the joining faces
- Closeness of faces and roll pressure
- Duration of the contact
- Rolling temperature
- Oxide formation on the joining faces
- Oxide fracture during rolling

1.2.1.3 Limitation due to edge cracking

The occurrence of edge cracks on the samples after a few passes limits the application of the ARB process. One of the reasons for edge cracking behavior is due to the continuous increase in hardness and strength of the material after each pass due to which the ductility of the material decreases. The second reason is the presence of precipitates that hinder the movement of dislocations, thus resulting in nucleation and

propagation of edge cracks due to dislocation pile up. In ARB process, 99% reduction of experimental material could be achieved, which is much larger than what can be achieved in one conventional pass or by forging without edge cracking. The large straining during reduction of material thickness is another cause of edge cracking during ARB. As the edge cracks further propagate in the material with subsequent ARB cycles, proper trimming of the edges, sometimes, becomes necessary to achieve more deformation without crack propagation. (Krallics and Lenard, 2004).

1.2.1.4 Advantages

The major advantages of this process against other high straining process are:

- It has the cabability of high productivity and the feasibility of bulk material production.
- It does not require any special machines, because the roll bonding is widely adopted in clad metal production.
- The materials processed by this route have almost homogeneous microstructure.
- It can be applied to materials with different crystal structures and to materials ranging from precipitation-hardened alloys to intermetallics and metal–matrix composites.

1.2.2 Equal Channel Angular Pressing (ECAP)

1.2.2.1 ECAP process

Equal-channel angular pressing (ECAP) is the most studied SPD processing technique (Valieve at al., 2006). It is an interesting and demandable method for modifying microstructure in producing ultrafine grained (UFG) materials. A schematic diagram of ECAP is shown in figure 1.4. In this process a rod/square shaped billet is pressed through a die constrained within an equal channel cross section, which is bent at

an abrupt angle. A shear strain is introduced when the billet passes through the point of intersection of the two parts of the channel. Since the cross-sectional dimensions of the billet remain unchanged, the pressings may be repeated to attain exceptionally high strains. The equivalent strain ε, introduced in ECAP, is determined by a relationship incorporating the angle (Φ) between the two parts of the channel and the angle (Ψ) representing the outer arc of curvature, where the two parts of the channel intersect. The relationship is given by (Meyers et al., 2005).

$$\varepsilon = \frac{N}{\sqrt{3}}\left[2\cot\left\{\left(\frac{\phi}{2}\right)+\left(\frac{\psi}{2}\right)\right\}+\psi\,\mathrm{cosec}\left\{\left(\frac{\phi}{2}\right)+\left(\frac{\psi}{2}\right)\right\}\right]$$

Where N is the number of the passes through the die.

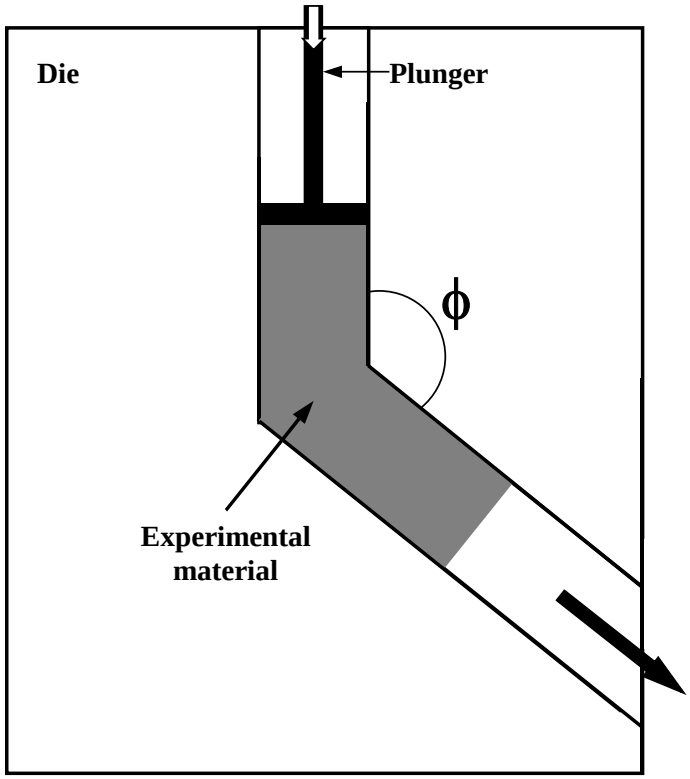

Fig. 1.4: A schematic diagram showing ECAP process

1.2.2.2 Processing routes in ECAP

There are four basic processing routes in ECAP and these routes introduce different shear routes during the pressing operation so that they lead to significant differences in the microstructures produced by ECAP (Nemoto et al., 1998; Horita et al., 2000; Furukawa et al., 2003). The four different processing routes are summarized schematically in Fig. 5. This shows that the sample is pressed without rotation (route A), the sample is rotated by 90^o in alternate directions between consecutive passes (route B_A), the sample is rotated by 90^o in the same sense (either clockwise or counterclockwise) between each pass (route B_C) and the sample is rotated by 180^o between passes (route C). Various combinations of these routes are also possible, such as combining routes B_C and C by alternating rotations through 90^o and 180^o after every pass, but in practice the experimental evidence obtained to date suggests that these more complex combinations lead to no additional improvement in mechanical properties of the as-pressed materials. Accordingly, for the simple processing of Bars or rods, attention is generally devoted exclusively to the four processing routes delineate in Figure 1.5.

1.2.2.3 Advantages

The following reasons make this method of high straining more preferable against other processes:

- It is a simple technique that is easily performed on a wide range of alloys, except the construction of the die.
- It can also be used to materials with different crystal structures and to many materials ranging from precipitation-hardened alloys to intermetallics and metal-matrix composites.
- Reasonable homogeneity is attained through most of the as-pressed billet provide the pressings of relatively large samples.
- The dimension of the billet remains unchanged, therefore, pressings may be repeated to attain exceptionally high strains.

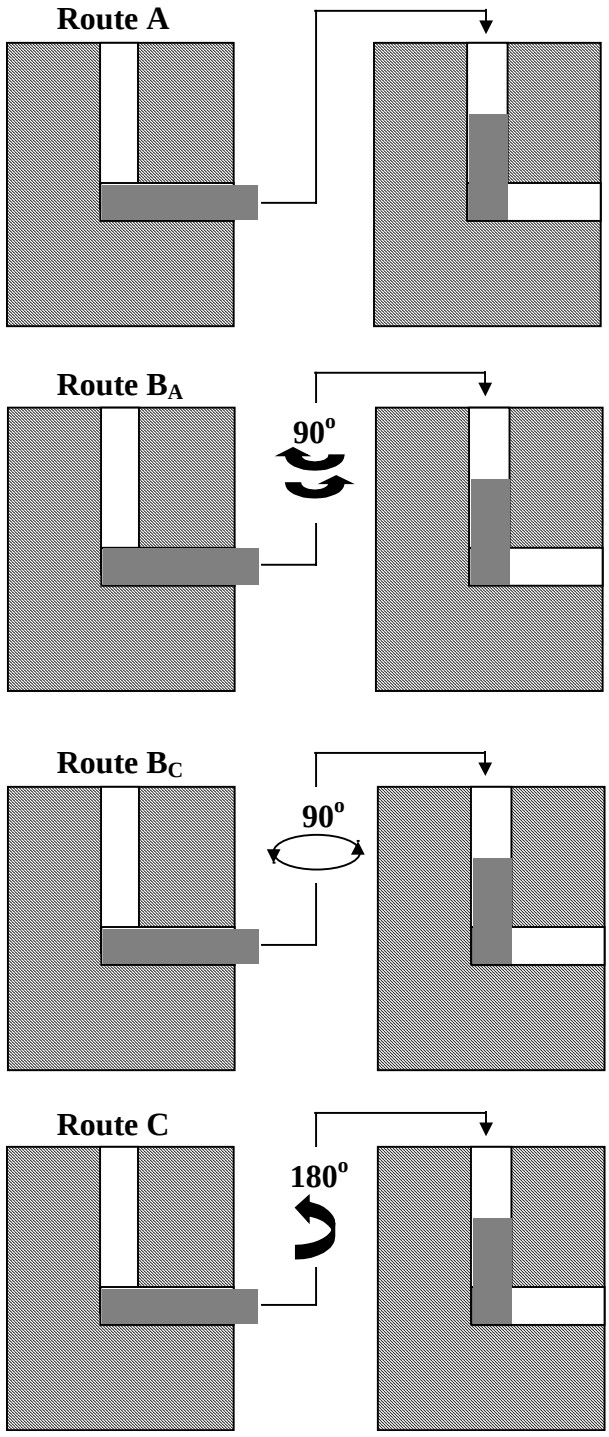

Fig. 1.5: The four fundamental processing routes in ECAP .

1.2.2.4 Experimental factors influencing ECAP

When materials are processed using ECAP, several different factors influence the workability and the microstructural characteristics of the as-pressed billets. These factors can be enumerated as follows: (Valiev et al., 2006)

- The angle between channels of the die (Φ)
- The angle of curvature (Ψ)
- The pressing speed of the punch in the die
- The material temperature
- Internal heating during ECAP
- Back pressure on the punch

1.3 Structural parameters of cold worked FCC metals

Since the present work has been undertaken to develop ultrafine-grained aluminum (Face Centred Cubic structure) by severe plastic deformation method and to examine the microstructure and mechanical properties by different characterizing tools, it is necessary to have an idea of the structural features of FCC metals and alloys. The structural features of SPD processed metals are quite complex and they are characterized not only by the formation of ultrafine grains but also the presence of non-equilibrium grain boundaries with a high density of extrinsic dislocations and vacancies, high lattice distortions, and possibly, changes in the local phase composition. The genesis of UFG structure produced by SPD techniques is not yet fully understood. While some authors relate them to in-situ recrystallisation (Lapovok et al., 2005), others have different opinions about the mechanism of UFG formation. Recently, a series of studies led by (Hughes and Hansen, 1997; Hughes and Hansen, 2000; Liu et al., 2002) showed that quantitative structural parameters of cold-worked FCC metals could be measured. This achievement has great technical importance due to the fact that the use of these quantitative parameters, modeling of the deformation microstructure can be performed. Dislocations generated by plastic deformation are not randomly distributed. They accumulate at dislocation walls, and the regions surrounded by these dislocation walls have relatively low density of dislocations. These dislocation walls may be classified into two types: (1) geometrically

necessary boundaries (GNB) and (2) incidental dislocation boundaries (IDB), due to their different formation mechanisms. When a grain is deformed, it is sub-divided into "cell blocks". The dislocation walls that separate cell-blocks are GNB. The GNBs accommodate the misorientation between neighboring blocks, which deform with different slip system combinations or by different shear amplitudes. Each cell-block is further divided into several cells. The geometrically necessary dislocations are generated in order to maintain continuity of the polycrystalline material. The dislocation walls that separate cells are IDB_S, which are formed as a result of statistical trapping of glide dislocations. As deformation proceeds, both the cell-blocks and the cell shrink in size, but the cell blocks shrink in size more rapidly than the cells do. Eventually, each cell becomes a cell-block.

1.4 The deformation physics of nanocrystalline metals processed by SPD

One of the important objectives of the present work is to identify interrelationship between the deformation mechanisms active during grain refinement process and to determine their influence on the mechanical behavior of UFG aluminum processed by accumulative roll bonding technique. There are various physical models related to interpretation of the physics of deformation of nanocrystalline metals and alloys. The first model was proposed by Pande et al. (Pande et al., 1993) and further developed by Armstrong and Coworkers (Armstrong and Hughes, 1999). According to this model the dislocations in the SPD processed metals and alloys are assumed to be in the center of the grain. As the grain size is reduced, the number of dislocations is eventually reduced to one and the stress amplification effect is lost. Figure 1.6a shows the individual dislocations (positive and negative) arrested at opposing grain boundaries and all dislocations pile-up at the grain boundaries.

The second model was proposed by Chokshi el at. (Chokshi et al., 1989). He predicted that the grain-boundary sliding plays a major role in nanocrystalline metals and alloys at ambient temperature. Simple grain boundary sliding is schemtically shown in figure 1.6b, and it could be responsible for negative slope in grain size domain d<10nm. In several recent experiments, the active development of grain boundary sliding was

revealed directly in UFG aluminium during deformation at room temperature through the use of atomic force microscopy and depth-sensing indentation testing (Chinh et al., 2006). The sliding contribution in these experiments was estimated as ~70% from measurements of the surface profiles around hardness indentation, thereby confirming the significance of sliding in the deformation of UFG structures. It is important to note that these data correlate closely with results demonstrating an increased strain rate sensitivity of the flow stress in UFG metals. The question remains why grain boundary sliding takes place in nanostructured materials produced by SPD at temperatures that are relatively low in comparison with the absolute melting temperatures of the materials. Thus, ambient temperature for pure aluminum corresponds to an homologous temperature of only ~0.32 T_m, where T_m is the absolute melting temperature of the material. Since grain boundary sliding is a diffusion-controlled process, it should occur preferentially at high temperatures where diffusion rates are reasonably rapid (Gifkins and Langdon, 1964). A possible explanation for the occurrence of sliding in UFG metals is that diffusion is more rapid in SPD-produced metals with highly non-equilibrium grain boundaries. Experiments have shown that in metals produced by SPD, the diffusion coefficient increases considerably, often by two or three orders of magnitude, and this is associated directly with the presence of non-equilibrium grain boundaries. Therefore, the grain boundary sliding is easier in these ultrafine-grained metals and develops during straining at lower temperatures leading to the possibility of observing increased ductility. It is well known in this connection that enhanced sliding in nanostructured metals may lead to superplasticity even at relatively low temperatures. The recent results obtained from modeling and experiments provide strong support for the proposal that new deformation mechanisms, that are not typical under the experimental conditions in conventional coarse-grained materials, may proceed actively in metals with UFG microstructures.

Plastic flow occurring under conditions of high temperature creep is one of the most internationally recognized mechanisms of deformation of a coarse-grained polycrystal. Following the approach developed many year ago by Bird and co-workers (Bird et al., 1969). They suggested that the steady state creep rate $\dot{\varepsilon}$, is generally expressed through a relationship of the form

$$\dot{\varepsilon} = \frac{ADGb}{kT}\left(\frac{b}{d}\right)^{p}\left(\frac{\sigma}{G}\right)^{n} \qquad (1)$$

where, D is the diffusion coefficient ($= D_0 \exp\left(-\frac{Q}{RT}\right)$ where D_0 is a frequency factor, Q the appropriate activation energy for the diffusion process, R the gas constant), G the shear modulus, b the Burgers vector, K the Bolzmann's constant, T the absolute temperature, d the grain size and σ the applied stress, P and n are the constants define as the inverse grain size exponent and the exponent respectively and A is the dimensionless constant.

Diffusion creep and grain boundary sliding are important flow processes associated with the presence of boundaries in polycrystalline materials. Diffusion creep occurs because there is an excess of vacancies along grain boundaries experiencing a tensile stress and a corresponding depletion of vacancies along grain boundaries experiencing a compressive stress. Vacancy flow takes place to restore the equilibrium conditions and this leads to an elongation of the grains along the tensile axis. There are two separate types of diffusion creep (1) Nabarro-Herring creep, where the vacancies diffuse through the crystalline lattice with n=1, p=2 and $D=D_l$ (lattice self diffusion coefficient) (Nabarro, 1950) and (2) Coble creep where the vacancies diffuse along the grain boundaries with n=1, p=3 and $D=D_{gb}$ (grain boundary diffusion coefficient).

As the grain boundary sliding refers to the relative displacement of adjacent grains under the action of the applied stress, sliding of irregularly shaped grains cannot occur without some form of accommodation mechanism, and in practice the sliding is accommodated by intragranular slip in the adjacent grains. If the grain size is large in comparison with the equilibrium subgrain size, λ ,subgrains are formed in the grains during creep, the dislocations pile up and climb into these subgrain boundaries and the rate of sliding is given by equation (1) with n=1, p=1 and $D=D_l$. However, if the grain size is smaller than λ as in superplastic materials, no subgrains are formed and the dislocations climb into the opposite grain boundary with n=1, p=2 and $D=D_{gb.}$ (Langdon, 1994)

In one another model Li (Li, 1963) recognized that grain boundaries could serve as sources of dislocations. Figure 1.6c shows a grain divided into two regions; a central core and the grain-boundary region called 'mantle'. The mechanical response of these two regions is different, with work hardening being more pronounced in the mantle. This is because the grain interiors are subjected to a more homogeneous state of stress, while in the mantle several other factors contribute to the increased hardening. The ratio between the volumes of these two regions is independent of grain size. There is a simple experimental evidence for the development of a mantle in the conventional polycrystalline domain (Zehetbauer et al., 1999). As the grain size is reduced, the mantle becomes proportionally larger, as shown in the right side of figure 1.6c.

Some literature shows the evidence of shear band formation (Wang, 2006). Figure 1.6d shows how neighbouring equiaxed nanograins can, upon rotating, create elongated grains that act as favored paths for plastic deformation. The major slip orientations and their rotation are marked in the grains by short segments in the centers of the grains.

The most important and significant results of the physical process that occur during plastic deformation of nanocrystalline metals have been obtained by molecular dynamic (MD) simulation. According to this model (Meyers, 2006), the grain boundaries act as both dislocation sources and sinks and continuous refinement of grain size leads to partial dislocation emission from grain boundaries as well as deformation twinning (Figure 1.6e). Even in metals with medium high stacking fault energies such as Al and Cu. As the grain size is reduced into the nanocrystelline range, dislocations can travel unimpeded throughout grains. Thus, dislocations emitted from one boundary can be annihilated at the opposite boundary (Asaro et al., 2003). The reduction in grain size of materials makes twinning more difficult and responsible for the flow of nanocrystelline FCC metals plastically.

1.5 Structure and properties of SPD Processed UFG materials

The grain size of the crystalline materials plays a significant and often a dominant, role on its mechanical and physical properties. The mechanical and physical properties of nanocrystelline or ultrafine-grained (UFG) materials differ from their

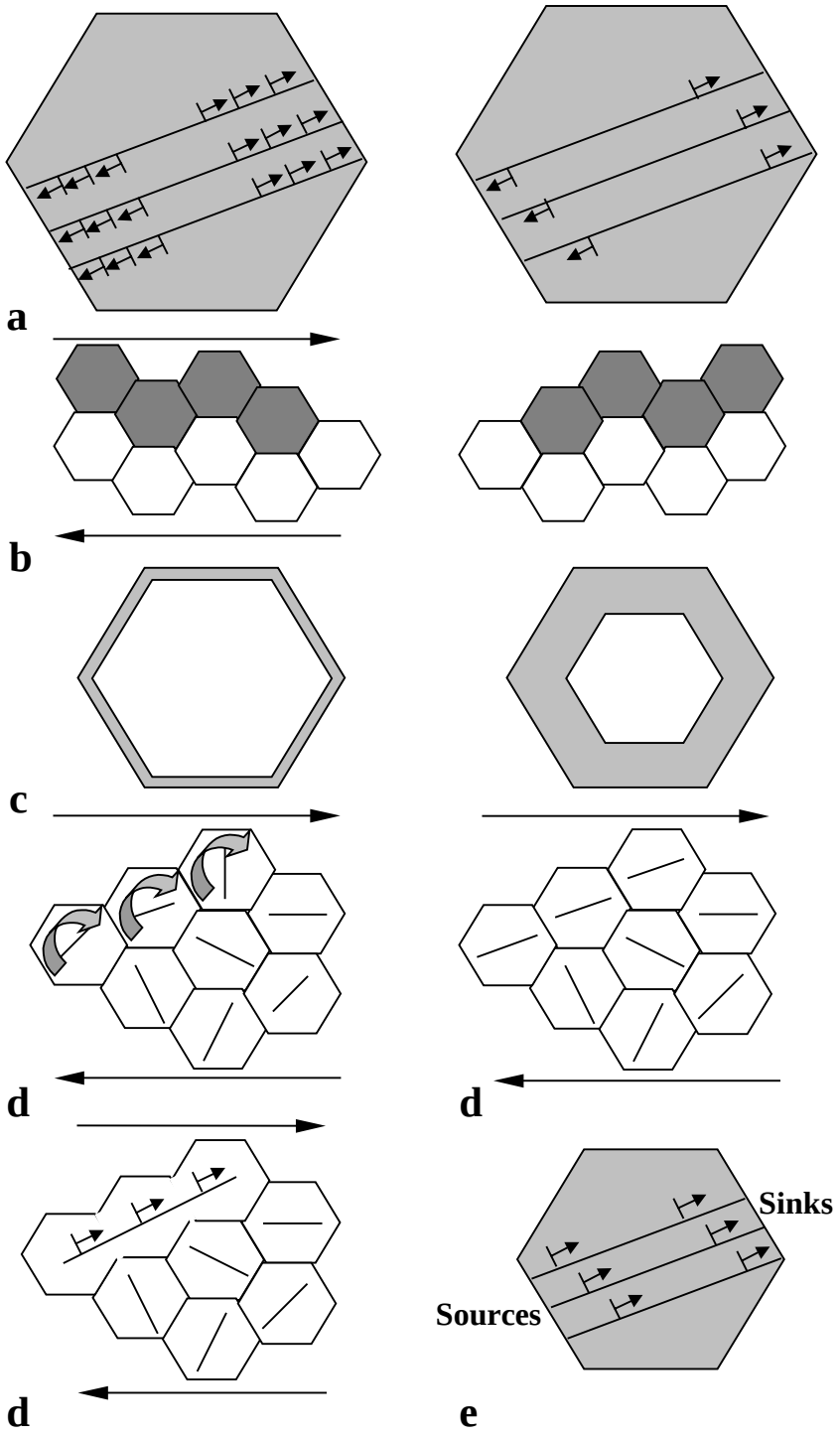

Figure1.6: Sketches of different deformation mechanisms: (a) pile-up breakdown; (b) grain boundary sliding; (c) core and mantle; (d) grain coalescence; (e) sequential generation in grain boundary sources and annihilation in grain boundary sinks.

coarse-grained (CG) counterpart. The strength of the polycrystalline materials is related to the grain size, d, through the Hall-Petch equation (Hall, 1951; Petch, 1953), which states that the yield stress σ, is given by

$$\sigma = \sigma_0 + k_y d^{-\frac{1}{2}} \qquad (1)$$

Where σ_0 is termed as the friction stress and k_y is a constant of yielding. It follows from Equation (1) that the strength increases with a reduction in the grain size. The average grain size achieved in pure metals using various SPD techniques usually lies in the range of ~150-300nm but in alloys it may be significantly smaller. For example, using High-pressure torsion (HPT) with the intermetallic Ni_3Al produced a grain size of 60 nm in Al-Ni alloys and in TiNi alloys processing by HPT led to total amorphization (Liao et al., 2004). The smallest grain size achievable by SPD cannot be smaller than the length scale of the precursor structure and thus of the dislocation cell size, which has an order of magnitude of some hundreds of nanometers. The most important features of SPD processing is that it leads to an exceptional grain refinement and thereby provides an opporunity to significantly enhance the properties of materials as well as to attain novel and/or unique properties. Table 1.1 shows the mechanical properties of various materials processed by SPD**.** One such unique property is the unexpected combination of high strength and high ductility. The specific processing of SPD and the associated simultaneous improvement of both strength and ductility is probably responsible also for the marked enhancement of fatigue strength and fracture toughness in UFG materials. As the grain size decreases to submicron-grained or nanocrystelline range, the fraction of grain boundary to matrix increases. This can cause the deformation mode to change from grain dominated in large grains to grain boundary dominated in small grain regimes. For smaller grain sizes, the empirical Hall-Petch relationship is expected to break down because it is based on dislocation pile up at the boundaries. As the grain size decreases, the number of "pile up" dislocations becomes smaller and, eventually, at a critical grain size, dislocations can no longer pile up at grain boundaries. Consequently, at this critical grain size, the yield stress no longer increases with decreasing grain size. It is believed that grain boundary processes, such as grain boundary sliding, grain rotation, or interface-

controlled plasticity, are some of the mechanisms that can control the deformation at these small grain sizes. For this reason, the dislocation source length and dislocation mean free path need to be considered in ultrafine grains (Anderson et al., 2003)

Another extraordinary property of UFG materials is their ability to exhibit superplasticity at high strain rates and at usually low temperatures, which provides an opportunity for the rapid superplastic forming of complex-shaped parts for use in the transportation and consumer product industries (Xu et al., 2004). Although most efforts to date have been directed toward improving the mechanical properties of structural materials processed by SPD, there is also recent evidence for other interesting developments. A general observation is that the increase in grain boundary area introduced by SPD can lead to enhancement in various kinetic properties of metallic materials. For example, it was found that the complex structure of SPD–processed materials might also result in multifunctional properties. For example, nanostructured TiNi alloy demonstrates an extraordinary combination of very high mechanical and functional properties including superplasticity and shape memory effect. Such a combination in the TiNi alloy is in stark contrast to its conventional coarse-grained counterpart. (Vorhauer et al., 2005). Not only does the nanometer grain size induce advanced mechanical properties but it leads also to enhanced soft magnetic properties due to an interaction of magnetic moments across the grain boundaries in these materials. Thus, the engineering of multifunctional materials is rapidly becoming a new direction in the science of SPD-nanomaterials.

1.6 Limitations of SPD methods of metals forming

Experimental data of UFG materials processed by severe plastic deformation indicates that they possess very high hardness and strength, 3 to 5 times that of their coarse grain counterpart, but their ductility, particularly uniform elongation in tension has been rather low and in the most cases nowhere close to that of the conventional metals and alloys (Koch, 2003). A similar tendency is well known for metals subjected to heavy straining by other process such as rolling or drawing. Strength and ductility are the key mechanical properties of any material but these properties typically have opposing

characteristics thus, materials processed by SPD methods may be strong but rarely ductile. Strengthening at the cost of ductility is not uncommon, and it is not surprising for a high-strength material such as UFG metals or alloys to be prone to instabilities upon large plastic deformation. The UFG materials processed via SPD has no capability to sustain a sufficient high rate of strain hardening and start necking soon after yielding, leading to a plunging tensile curve almost from the outset, which is a major short coming of UFG materials. These drawbacks could be an insurmountable hurdle in bringing bulk UFG materials from laboratory to commercialization. Despite this limitation, it is important to note that the SPD processing leads to a reduction in the ductility, which is generally less than in more conventional deformation processing technique such as rolling, drawing and extrusion.

The low ductility is caused by the low strain-hardening rate, which cause early-localized deformation in the form of necking. In general, two factors are responsible for the low or zero strain-hardening rate.

- A high density of dislocations already exists in nanostructured materials processed by SPD and the density quickly reaches saturation upon further deformation. Once the saturation is reached, dislocations no longer accumulate inside the grains and strain-hardening rate becomes zero.

- In the grains with very small diameters e.g. <100 nm dislocations are emitted from a grain boundary segment and disappear into another grain boundary segment on the opposite side of the grain without accumulating inside the grain. The saturation density of dislocation is determined by a balance between the dislocation generation rate and the recovery rate, and this saturation density is expected to be higher at lower deformation temperature and higher strains.

Table 1.1 Mechanical Properties of initial and SPD processed materials

Material	Processing technique	Temp. (°C)	Ultimate tensile strength (MPa)		Elongation (%)		Ref.
			Initial	Final	Initial	Final	
Al 1100	ARB	200	80	300	44	6	Saito et al. 1998
A 1100	ARB	200	50	250	30	3	Xing et al. 2001
A8011	ARB	200	50	150	48	10	Xing et al. 2001
AA8011	ARB	RT	35	160	42	18	Xing et al. 2002
AA8011	ARB	200	35	155	48	10	Xing et al. 2002
Ultra low carbon steel	ARB	515	183	695	75	4	Krallics et al. 2004
IF Steel	ARB	500	274	751	57	6	Tsuji et al. 1998
Al-Mg(5083) alloy	ARB	200	319	551	25	6	Saito et al. 1999
Ti	ECAP	500	1000	1400	-	-	Wang et al. 2004
Cu	ECAP	RT	120	450	46	4	Valiev et al. 2002
Cu	ECAP	200	120	400	-	-	Torre et al. 2004
Al-10.8Ag	ECAP	RT	175	275			Horita et al. 2005
Al 3004	ECAP	RT	80	400	32	14	Yu et al. 2004

1.7 Possible methods to improve ductility of nanostructured metals and alloys

The high strength and good ductility in several bulk ultrafine-grained metals produced by severe plastic deformation have received special interest (Valieve, 2000 and Wang et al., 2006). Several articles recently reported the UFG materials maintaining both high strength and adequate ductility. It is important to consider the various approaches that were used in these investigations.

- The non-equilibrium state of grain boundaries have been proposed as a mechanism to enhance ductility. It has been argued that such boundaries provide a large number of excess dislocations for slip and can even enable grains to slide or rotate at room temperature leading to a significant increase in the strain hardening exponent and ductility.
- Decreasing the strain rate in order to sustain more plastic strain prior to necking is a way to increase ductility.
- The availability of a bimodal (a mixture of two or multi- phases with varying size scale and properties) distribution of grain size leads to a considerable increase in ductility. In one of the studies, nanostructured copper was produced through a

combination of ECAP and subsequent rolling at the low temperature of liquid nitrogen prior to heating to a temperature close to ~450 K. This procedure gave a bimodal structure of micron-sized grains, with a volume fraction of around 25%, firmly fixed in a matrix of nanocrystalline grains. The material produced in this way exhibited an extraordarily high ductility but also retained a very high strength. (Wang et al., 2002)

- The presence of nanoparticles of a second phase increases ductility of the UFG materials. The availability of nanoparticles of second phase in the nanostructured metallic matrix modify the shear-band propagation during straining and thereby increasing the ductility (Lu et al., 2004).
- Both the strength and ductility of a material processed by SPD can be improved by performing mechanical tests at lower temperatures (Tsuji et al., 2006)

The conclusion of the literature available related to SPD reveal that the grain refinement by SPD can lead to a unique combination of strength and ductility in metallic materials. Such superior mechanical properties are highly desirable in the development of advanced structural materials for the next generation. However, the achievement of these properties is associated with further treatment to create specific microstructure that is responsible to improve the ductility of the material.

****

CHAPTER-II

Experimental Details

As the present work is aimed at the development of ultrafine-grained aluminium 1100 alloy by severe plastic deformation, the primary objective is to refine the grain of aluminium 1100 alloy from micrometer to ultrafine size by accumulative roll bonding process, their microstructural characterization and property evaluation. Therefore, in this chapter, various experimental procedures undertaken to carry out ARB processing and materials characterisation have been given.

2.1 Selection of material for SPD

In this study, a commercial purity aluminium 1100 was used in the test whose chemical composition is shown in Table 2.1.

Table 2.1: Chemical composition of the 1100 Aluminium (wt.%)

Si	Fe	Cu	Mn	Mg	Ti	B	V	Ni	Al
0.11	0.56	0.11	0.01	0.02	0.02	0.0007	0.011	0.003	balance

2.2 Sample preparation and procedure for ARB

The commercial pure aluminium (1100) strips, nominally 1.65 mm thick, were cut into samples of 35 mm width and 150 mm length. The two joining surfaces of the stips were cleaned and roughened using a wire brush, removing a thin layer and creating somewhat random surface. After brushing, the surfaces were cleaned using acetone. The strips were then joined on the roughened surfaces, while holding them in a vice to assertion that they lie flat against one another, and the leading and trailing edges were tightened with a steel wire. The leading edge was tapered to ease entry to the roll gap.

Then the strips were rolled dry to a nominally 50% reduction, at a velocity of 3 $m.min^{-1}$ of rolling speed, creating strain rate of approximately 10 per second in a 12 kW, 2/4 high, Ameco Laboratory rolling mill with a maximum rolling speed of 45 $m.min^{-1}$ and maximum roll force of 500 KN. The roll diameter is 300 mm. A photograph of the rolling mill used in the present study is shown in figure 2.1. This procedure defines one cycle/pass of ARB. No lubrication was used during the passes. After each pass, a sample for subsequent testing was cut from the strip and remaining strip was cut into two halves and, the same procedure was repeated again. The ARB process was repeated up to 7 passes. The rolled strips were visually inspected for appearance of edge cracks and for successful bonding. The experiments were stopped when cracking of the edges became pronounced. All the ARB experiments were carried out at room temperature. Rolling at high temperature is advantageous for joinability and workability, though too high temperature would cause recrystallisation and cancel the accumulated strain. Therefore, we restricted to room temperature rolling only.

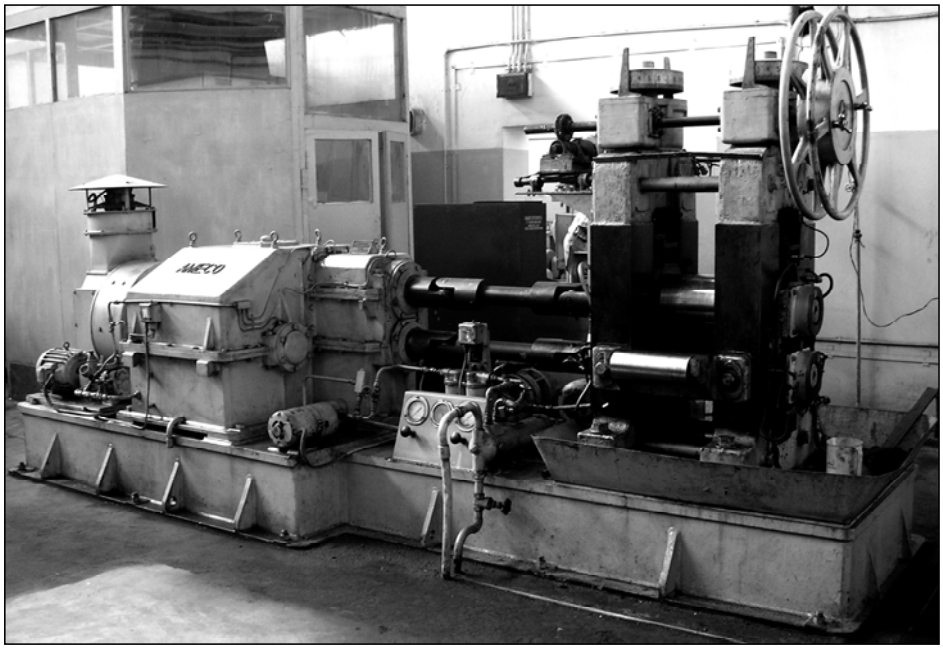

Fig. 2.1: Photograph of the rolling mill used in the present work.

2.3 Sample preparation for microstructural analysis

For the purpose of examining the bonding quality the samples from all the ARB passes were cut, mounted and metallographically polished with successively finer grades of emery papers and with silvet cloth using alumina powder of 0.3 micron grain size. The final polishing was done using diamond paste. The polished samples were etched with modified Keller's reagent (2% HF, 3% HCl, 95% H_2O). Microstructure investigations were carried out on ***optical microscope*** of maximum 1500 magnification with image analyzer for optical analysis.

Specimens for ***transmission electron microscopy*** were prepared from the deformed samples of 1^{st}, 3^{rd}, 5^{th} and 7^{th} pass by cutting several small samples of 3 mm diameter parallel to the rolling plane. The samples were mechanically thinned to a final thickness 100 μm followed by ultrasonic cleaning and twin-jet electro-polishing using a 400 ml CH_3OH + 40 ml $HClO_4$ solution at –15 ^oC at a voltage of 20V. Then the samples were examined in a PHILIPS CM 200 CX transmission electron microscope (TEM) operated at 200kV and at 10^{-9} mbar vacuum.

Specimen for ***atomic force microscopy*** were prepared from 1^{st}, 3^{rd}, 5^{th} and 7^{th} pass of ARB processed sheets. The samples were with 6 mm thickness and 3 mm width. The longitudinal section of the samples was metallorgraphically polished following the procedure as mentioned above. The polished samples were electro-polished using 700 ml Ethanol + 200 ml perchloric acid + 100 ml glycerin solution at 20 V for 60 s. After the electro-polishing step, samples of 5^{th} and 7^{th} pass were etched using dislocation etchant (2 parts solution of 65 ml HCl + 35 ml HNO_3 and 5 part solution 49 ml HF + 51 ml water) at –15^oC. The microstructure investigations were carried out on Atomic force microscope model SPA 400 (Seiko Instrument Inc.). The dislocation etched samples were also examined under scanning electron microscope so as to have an idea of the joined interfaces. Dislocation etching is supposed to reveal the cracks more prominently.

The fractured surfaces generated after tensile testing give an idea of the fracture mode of the samples as well the fracture mechanism. As the ARBed materials are made of several layers, the fracture behaviour was important to study so as to have the idea of

interface behaviour during straining. Therefore, as-fractured surfaces were examined under ***scanning electron microscope*** JSM 840 C.

2.4 Mechanical testing

Two sets of samples of 0 to 5th pass ARBed material were prepared following standard dimensions as given in figure2.2 by conventional machining. These samples were tested on an INSTRON machine at room temperature to measure several properties like ultimate tensile strength, % elongation etc. The strain rate applied to the samples was 10^{-4} s^{-1}. The Vickers hardness of each pass of ARBed samples were taken on both the cross-section and surfaces using a Leica Microsystem Vickers Micro Hardness Tester (automatic) using a load of 1 kg.

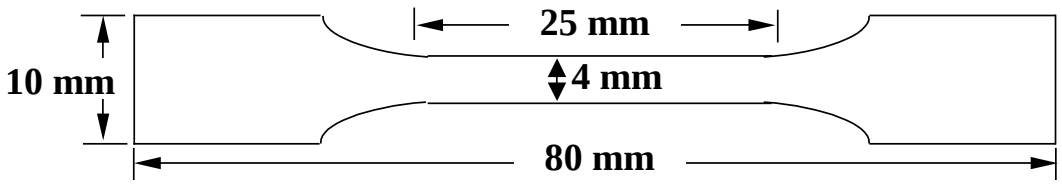

Fig. 2.2: Schematic of tensile test specimen

2.5 Texture Measurement

ARBed samples are having different number of layers. To understand that, textural evolution was carried out at two thickness levels: at the surface and at the middle. Samples for the mid-section were polished in emery paper from one side of the specimen. For all sample stages, crystallographic texture was determined by measuring {111} pole figures ($5^o \leq \alpha \leq 75^o$) by means of an automated texture goniometer with Co-Kα radiation.

****

CHAPTER-III

Results

The results obtained from the present work are presented and described in this section. As the main objective of the present work is to establish a qualitative relationship between the microstructural evolution in ARB process and their effect on mechanical properties, we present here the results in terms of microstructural characteristics and the change in mechanical properties thereof. The experimental observations for seven cycles of ARB is shown in Table 3.1. A total true strain of 5.83 could be introduced in the roll bonded layers after seven passes. The reduction varied between 50-60% in each pass and has been observed to suffice for the refinement of the grains of the experimental sheets up to ultrafine size and to achieve good bonding between the interfaces. A thickness reduction of 99.12% could be achieved after seven passes of ARB.

Table 3.1 Process parameters and the experimental observation

Sr. No.	Pass	Initial Stack (mm)	Final Stack (mm)	No. of Layers	Initial layer Thickness (mm)	Final layer Thickness (mm)	% Reduction	True strain
1	0^{th}	1.65	---	1	1.65	---	---	0.00
2	1^{st}	3.30	1.40	2	1.65	0.700	57.58	0.99
3	2^{nd}	2.80	1.45	4	1.40	0.363	74.11	1.75
4	3^{rd}	2.90	1.50	8	1.45	0.188	87.07	2.51
5	4^{th}	3.00	1.45	16	1.50	0.091	93.96	3.35
6	5^{th}	2.9	1.35	32	1.45	0.042	97.09	4.23
7	6^{th}	2.50	1.20	64	1.25	0.019	98.50	5.17
8	7^{th}	2.40	1.35	128	1.20	0.011	99.12	5.83

3.1 Interface characteristics

The optical and SEM micrographs of longitudinal cross-section of as ARBed samples of different passes are shown in Fig. 3.1 and Fig. 3.2 respectively. This exercise was undertaken to have an idea of the bonding characteristics and oxide entrapment during bonding. The optical micrographs do not give a clear picture of bonding line between the layers of samples. The interfaces are visible with discontinuous line in white contrast. The discontinuous appearance of the interfaces creates confusion about the quality of the bonds. So it is very difficult to comment on the quality of the bond whether it is properly bonded or not. However, the number of discontinuous lines (i.e. interfaces created) matched well with the expected number of interface in each pass. To avoid the ambiguity created in examining the bond quality, the samples were dislocation etched (as mentioned in the section 2.3). The scanning electron microscopy of dislocation etched samples show a morphological change in comparison to the optical micrographs, due to the fact that this etchant attacked preferentially at the highly strained areas or cracks. The initial specimen (0^{th} pass) showed a typical recrystallized structure with almost equiaxed grains, and its mean grain size was ~ 5 μm (Fig. 3.2a). The interfaces introduced in the second cycle, dividing four metallic layers, specimen is clearly seen in Fig. 3.2b. The interfaces in the sample after 2^{nd} pass reveal clearly that the bonding between layers is not continuous. This indicates the presence of some oxide particle adhering to the cleaned surface joined. The presence of such oxide particles restricts proper bonding between metallic layers. However, two nascent surfaces are properly joined leaving no trace of visible two layers, resulting in discontinuous interface. It has been observed and also obvious from the figure that the interface created in the first pass (two outer interfaces) is qualitatively better compared to that created in the first pass (middle interface). The absence of oxide particle gives rise to a good bonding at the interface. After three cycles of ARB (i.e. 8 layers), it becomes difficult to recognize the interface from the first pass (Fig. 3.2c). And also, the bonding seems to improve at the interfaces created in earlier passes. It is also observed that the size of oxide/debonded regions change in different

pass interfaces, which may be attributed to the experimental conditions of cleaning carried out before each pass. Similarly, the 4th pass sample shows distinct 16 metallic layers of approximately 100 μm thickness (Fig. 3.2d). This satisfies well the theoretical calculation for the layer thickness after 4th pass. A little consideration given to the above micrograph emphasizes that the materials becomes a composite with distribution of oxide particles in the Al matrix.

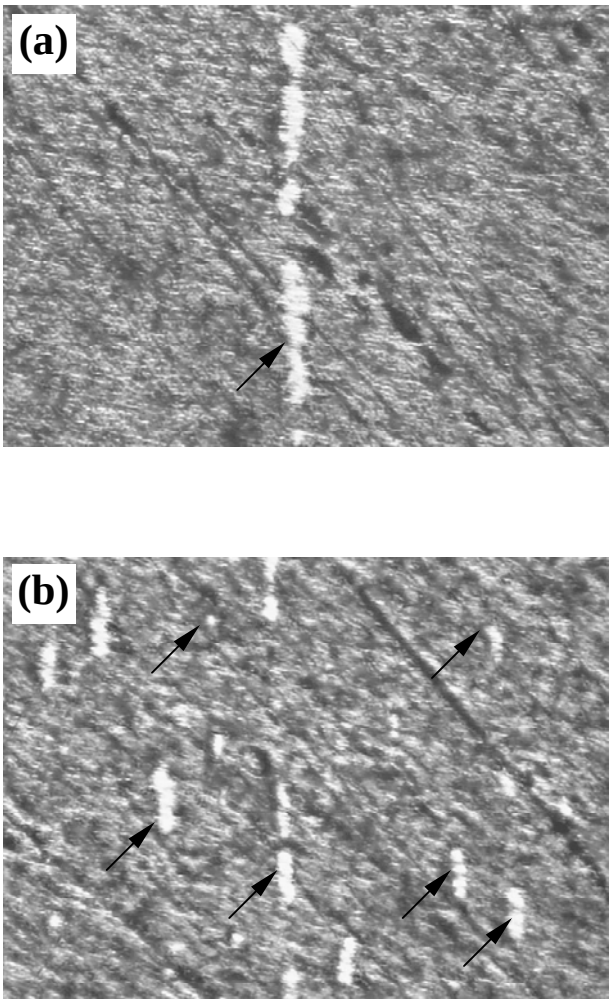

Fig. 3.1: Optical micrographs of 1st and 4th pass ARBed material showing joined Interfaces (a) 1st pass and (b) 4th pass.

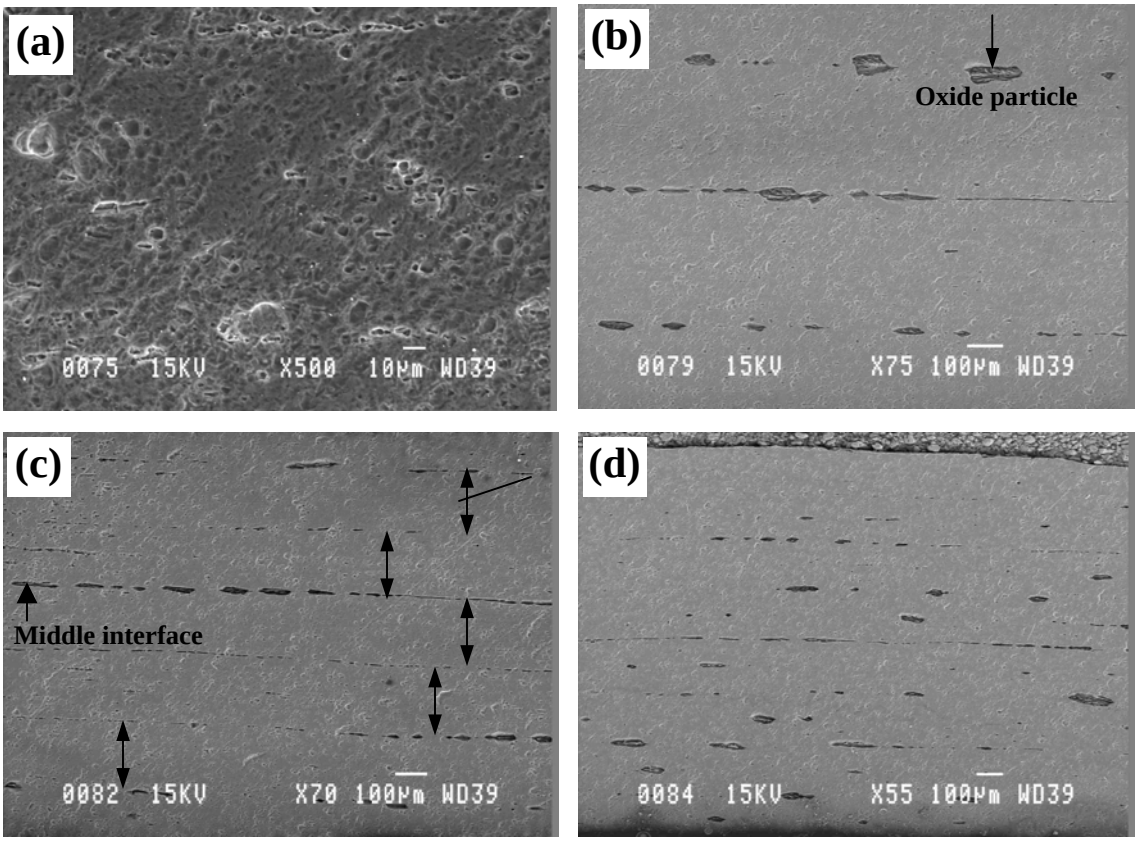

Fig. 3.2: SEM micrographs of longitudinal cross-section (a) showing initial material microstructure and (b, c and d) showing interfaces of 2^{nd}, 3^{rd} and 4^{th} pass respectively.

3.2 Microstructural evolution

3.2.1 Transmission electron microscopy

The property of the ARBed materials depend to a large extent upon the microstructural features generated after each pass. As the basic purpose of ARB is to develop ultrafine grained materials, it is expected that the microstructural change would occur in each subsequent passes during processing. Therefore, a few of the ARBed samples from 1^{st}, 3^{nd}, 5^{rd} and 7^{th} pass were examined under transmission electron

microscope to evaluate the structural development and mechanism of grain refinement during this process.

The TEM micrographs of the samples from 1st, 3rd, 5th and 7th passes are shown in figs. 3, 4, 5 and 6 respectively. All the micrographs have been taken in the rolling plane of the samples. The micrographs of 1st cycle specimen, which experienced a 57.58% reduction in thickness at a true strain 0.99, reveal dense dislocation walls/microbands having an angle of about 40° with the rolling direction, as shown in fig. 3.3a. The microstructure of this cycle of ARB primarily showed subgrain structure with high dilslocation density. The average grain size after this cycle of ARB is approximately 1.5 μm. Fig. 3.3b shows single net SAD pattern which indicate that the area have very low misorientation. The dislocation interaction is very high and the density is found to increase with increasing grain size. Large grain seem to divide into several subgrain (fig. 3.3b and c). Almost every grain displayed dislocation tangled within the grain (figure 3.3d). Formation of boundaries fringes is visible in this pass but there are many dislocation attached to the boundaries (fig. 3.3e).

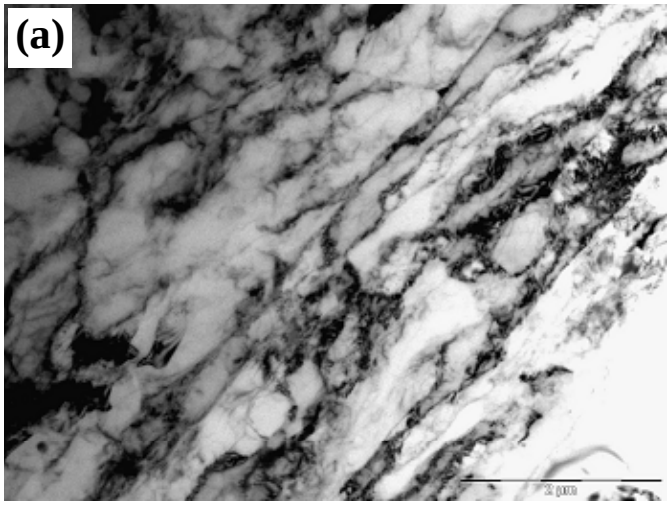

Fig. 3.3: TEM micrograph of 1st pass sample showing (a) elongated grains in rolling plane.

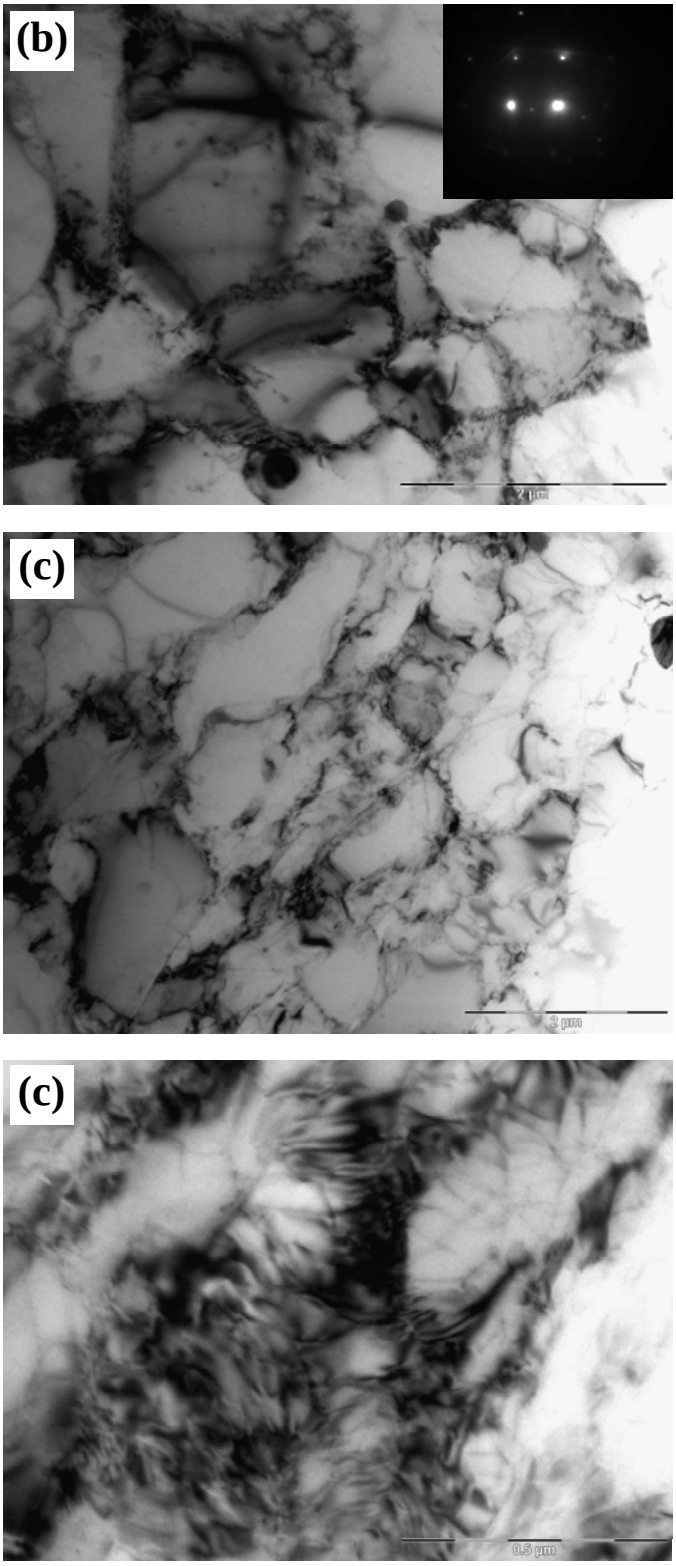

Fig. 3.3 (contd.): TEM micrographs of 1st pass sample showing (b & c) subgrain structure and (d) high dislocation density.

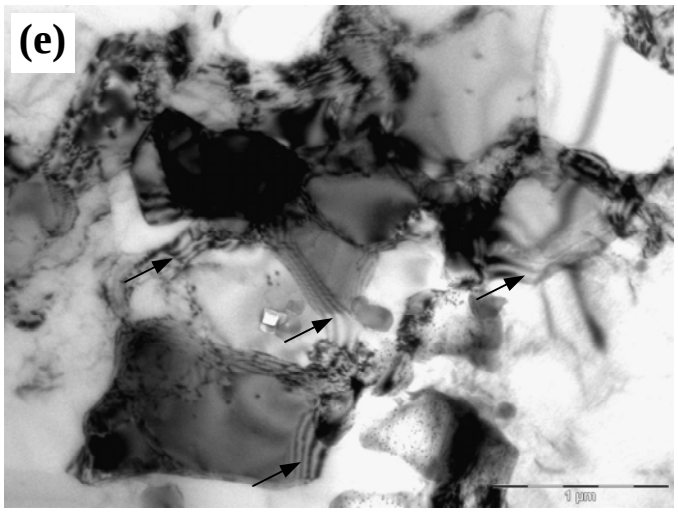

Fig. 3.3 (contd.): TEM micrographs of 1st pass sample showing (e) grain boundary fringes.

The micrographs of 3rd cycle of ARB (87.5% reduction in thickness of the initial experimental material with 1.75 true strain) are shown in the Figure 3.4. Figure 3.4a shows ultrafine grains with average diameter of less than 1μ. This indicates that ultrafine grains begin to form from this pass i.e. at a true plastic strain of 1.75. The dislocation density within each fine grain is very low, the ultrafine grains show almost equithickness fringes at their boundaries, which suggest that those boundaries are well-developed ones and have large misorientations, although they have irregular shapes. Figure 3.4b shows nearly single net SAD pattern, though scattering of the spots can be recognized to some extent and most of the specimen still has subgrain structure at this stage. Etch-pits can be clearly seen at grains surfaces, which are the source of dislocations. Pile-up of dislocations on the boundary of grain is also visible and tightly packed near the boundary and forms sessile (immobile) locks of dislocation. This kind of fringes may also be possible in the case of overlapped grains, where fringes are created due to constructive and destructive diffraction in the overlapped region. The dislocation locks are important because they are easily created at the intersection of active glide planes and then block the traffic of other mobile dislocation on or near these planes, thus hardening of the

metals. Figure 3.4c shows sharp break in dislocation line moving it out of glide i.e. jogs and sharp break in dislocation line not moving it out of glide plane i.e kinks. These jogs and kinks are created at the intersection of dislocations. Figure 4d shows formation of extremely fine subgrains of approximately 400-500 nm in a large grain of 2.5 μm. It has been observed that a large number of grains transform to subsgrains, whereas, many of the grains still remain with high dislocation density at grain boundaries.

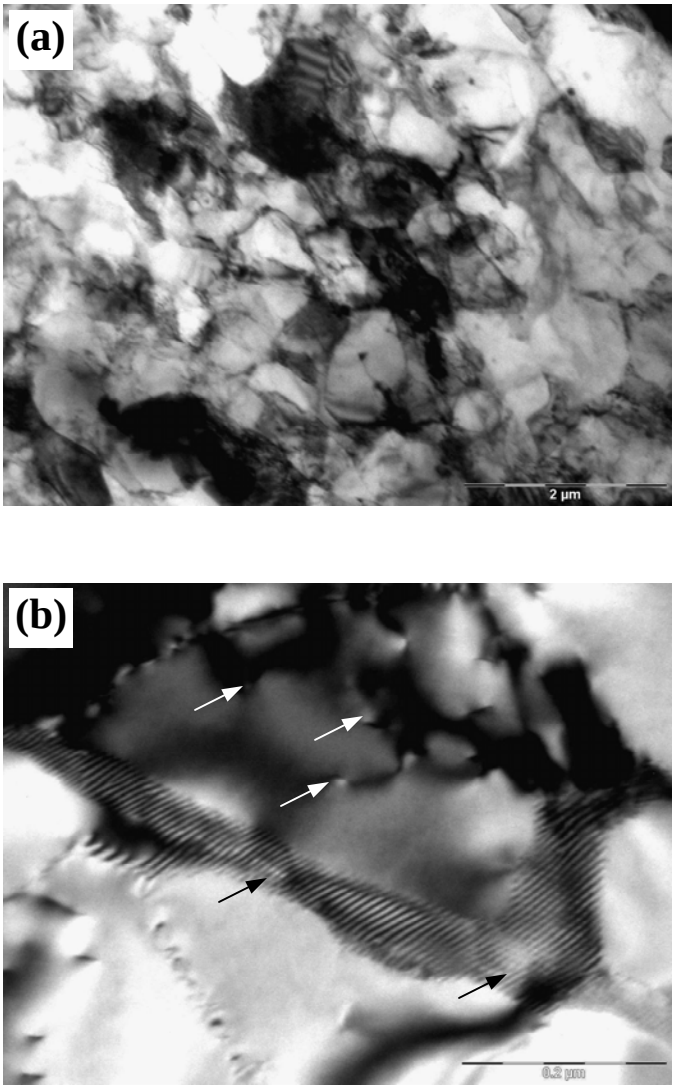

Fig. 3.4: TEM micrographs of 3rd pass sample showing (a) ultrafine grains and (b) etch pits on the grain surface and dislocation pile up at grain boundary.

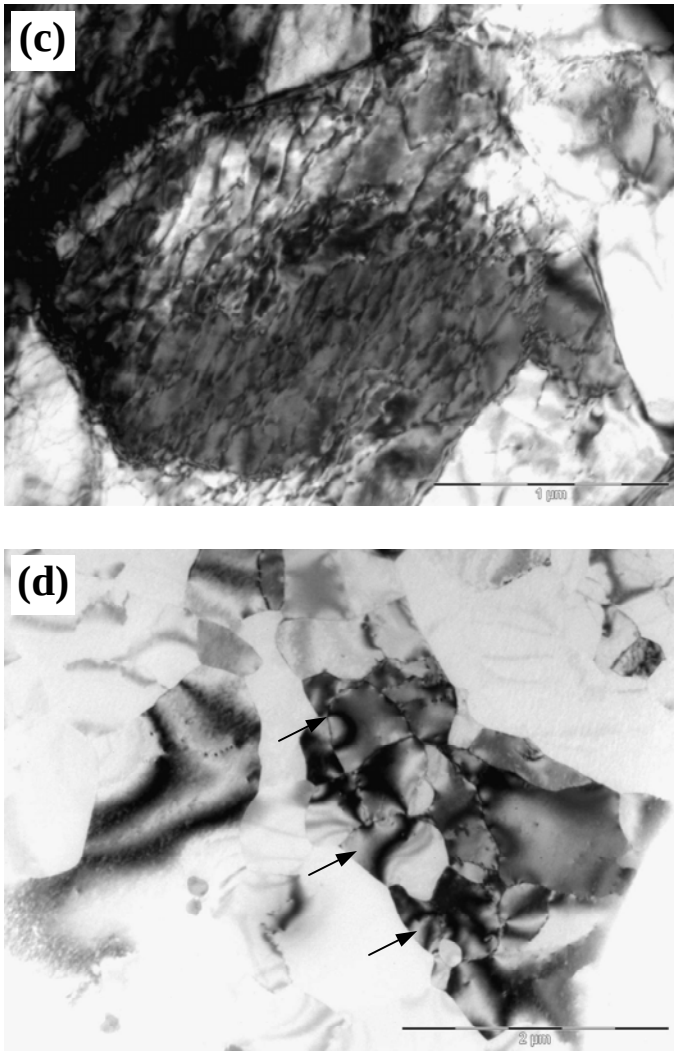

Fig. 3.4 (contd): TEM micrographs of 3rd pass sample showing (c) dislocation network within a large grain (d) well developed subgrains.

After the 5th cycle of ARB (97.09% reduction in thickness at strain 3.35) ultrafine grained structure become more dominant and some regions showed scattered diffraction pattern. Figure 3.5a shows the existence of large misorientations. That is, the ultrafine grains in those regions are polycrystals. However, some parts still has less misorientation at this stage, Although some fine grains could be observed even in these regions. It should be emphasized that the formation of the ultrafine grains is regionally

inhomogenous in the highly strained materials. The fraction of the ultrafine grained regions increases in 5th cycle, ultrafine grained structure become more dominant and some regions showed highly scattered diffraction pattern. Grains with clear prismatic boundary fringes can also be seen, which is evidence of massive dislocation annihilation. Figure 3.5b shows the transformed low angle boundaries into high angle grain boundaries. And also, the subgrains are free from dislocations. The low angle boundaries generated in each pass seemed to change to high angle boundaries in subsequent passes.

After 7 cycles of ARB (reduction 99.12%) at true strain 5.83, the whole volume of the material was filled with the ultrafine grains homogeneously (figure 3.6a). However, the grain size did not show any significant decrease in size as compared to earlier passes. It seems that some new mechanism is activated at this stage, which led to fast dislocation annihilation reducing the dislocation density. Some contours within the grains are also seen, which indicates high stress energy regions. Figure 3.6b show the dislocation structure similar to that observed after the first pass i.e. dislocation segregated at the grain boundaries. Before the 1st pass the grain size was around 5 μm, therefore, high dislocations density could be observed within the grains. Whereas, the starting grain size for the 6/7 pass was in the range of 500-800 nm, which would have led to faster dislocation annihilation at the grain boundaries. The co-existance of dislocations and dislocation loop debris was an evidence of dislocation generation and annihalation occuring simultaneously at large plastic strains. Figure 3.6c shows fine subgrains of around 400-500 nm size even after 7th pass. However, this behaviour was not very dominant in 7th pass material compared to those observed in the 3rd and 5th pass.

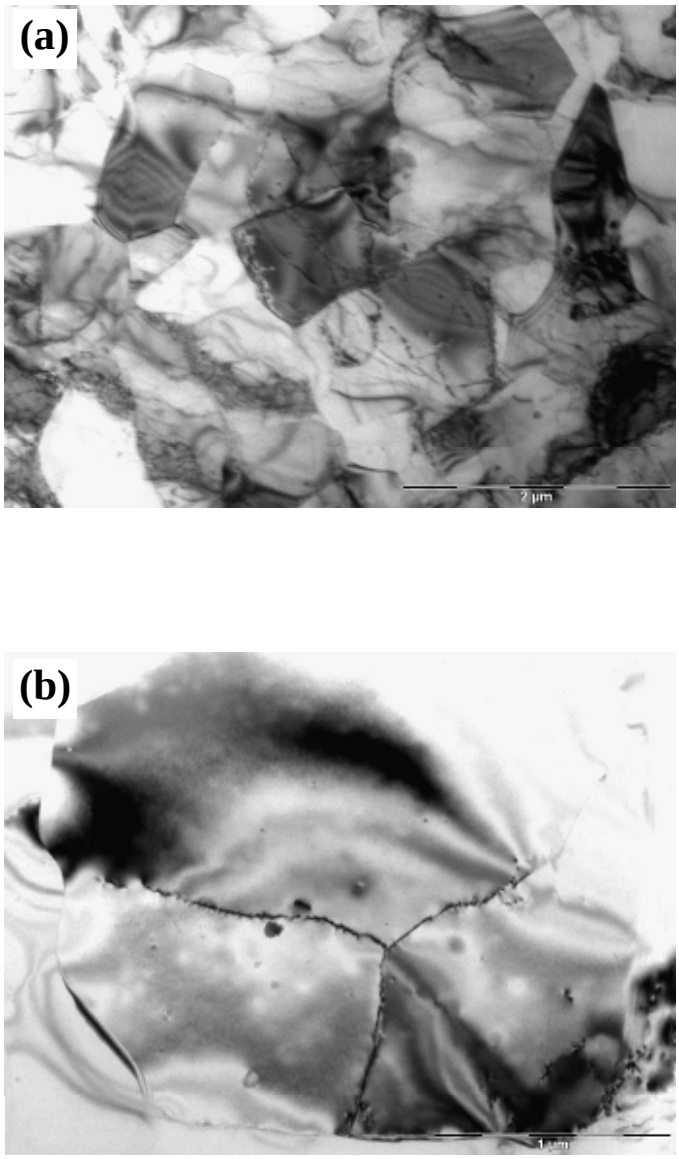

Fig. 3.5: TEM micrographs of 5th pass showing (a) ultrafine grains with prismatic fringes (b) subgrains completely free from dislocations.

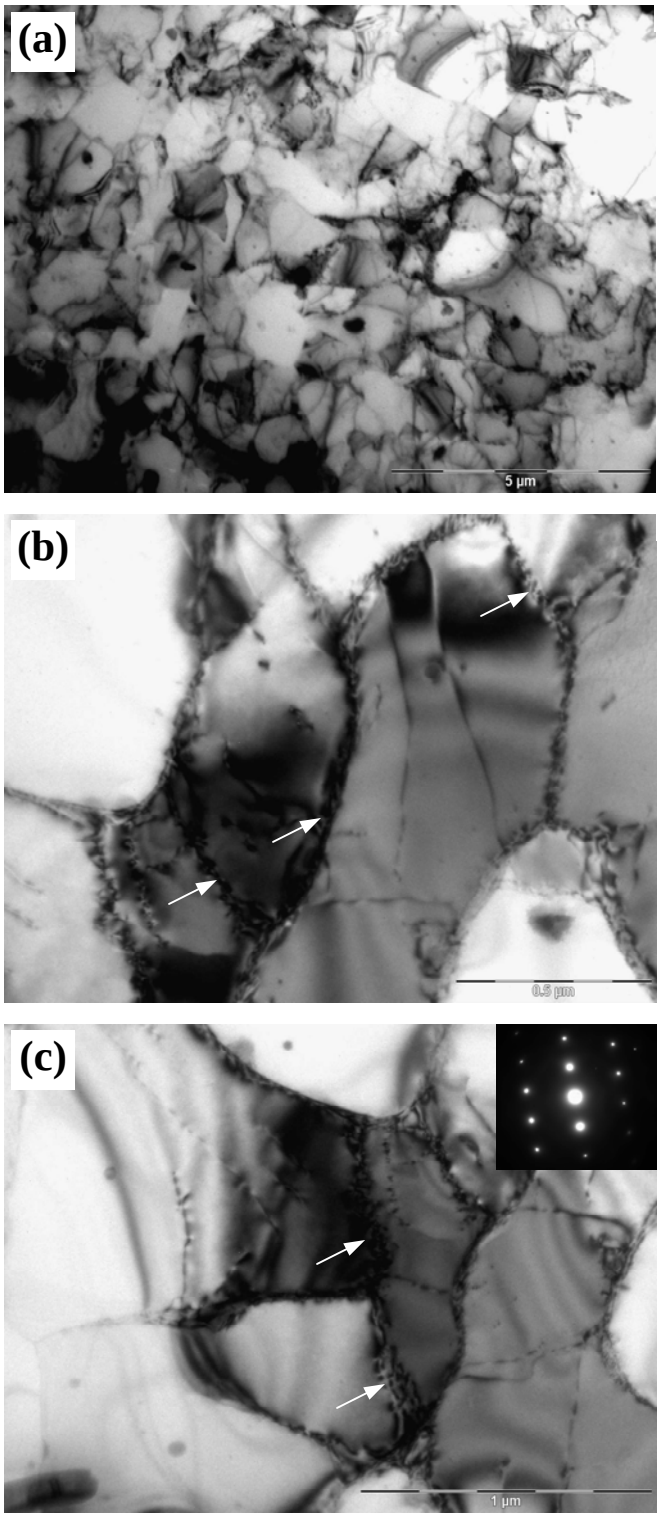

Fig. 3.6: TEM micrographs of 7th pass showing (a) ultrafine grains with some high stress energy contours within the grain (b and c) subgrain structure with dislocation concentration at grain boundaries.

3.2.2 Atomic force microscopy

The AFM micrograph on the longitudinal cross-section after 5^{th} and 7^{th} cycle of ARB samples are shown in figure 7 and 8 respectively. Figure 3.7a shows the transformation process of grain into subgrain and vice-versa, the mixture of stable and unstable boundaries can be seen clearly. Some grains in the figure are well developed with stable and high misorientation and some grains are divided into subgrains with unstable boundaries. The subboundaries coalesce to form a stable boundary. The coalescence of subgrains is associated with "unraveling" of unstable subboundaries and the passage of dislocations from them into nearest more stable sub-boundaries. An indirect evidence to this is that the disappearance (unravelling) of a boundary usually begins in direct contact with stable sub-boundaries. It is expected from the results of these observations in AFM that unravelling boundaries are charecterised by a lower dislocation density than stable ones. The cross slip plays an important part in forming favourable conditions for coalescence of sub-grains. Figure 3.7b shows ultrafine grained structure near the interface. The grain size in the interfacial region is expected to be highly refined due to the fact that these regions experience a high shear strain during ARB, compared to the middle of the layer. The average of grain size in the figure is 200 nm. The ultrafine grains completely converted into nanocrystalline grains in further straining of the specimen, it can be seen in the AFM figure 3.7c, which have grains of diameter about 177 nm. It is also found that the grain boundaries in the 7^{th} pass specimen are more stable than that of the 5^{th} pass specimen.

3.3 Evaluation of Mechanical properties

3.3.1 Hardness measurements

The Vickers hardness on ARB processed samples was measured using a load of 1 kg. Figure 3.8 shows the graphical presentation of the data of the hardness of the samples from 0^{th} to 7^{th} cycle of ARB both at the longitudinal cross-section and the surface of the ARBed samples. The surface hardness of the material increased from 17 Hv in the 0^{th}

pass to a maximum value of 43.72 Hv after 7th pass. The hardness on the surface of the material increases gradually against increasing strain value. However, an abrupt decrease after 6th pass and an increase thereafter is a remarkable observation. The maximum value of hardness on the cross-section is 36 Hv. At the cross-section also the same trend is observed. However, the hardness at cross-section is lower primarily after 6th and 7th pass. This indicates that this behaviour is due to the materials constitution. The variation in hardness of the ARBed material is dependent on several factors and one of them is the materials homogeneity. The existence of oxide particles and poor bonding at the interface may change the bulk hardness of the materials. A low value at cross-section after 6th and 7th pass may be attributed to the large number of interfaces created in the materials. However, this difference is not observed in the initial material.

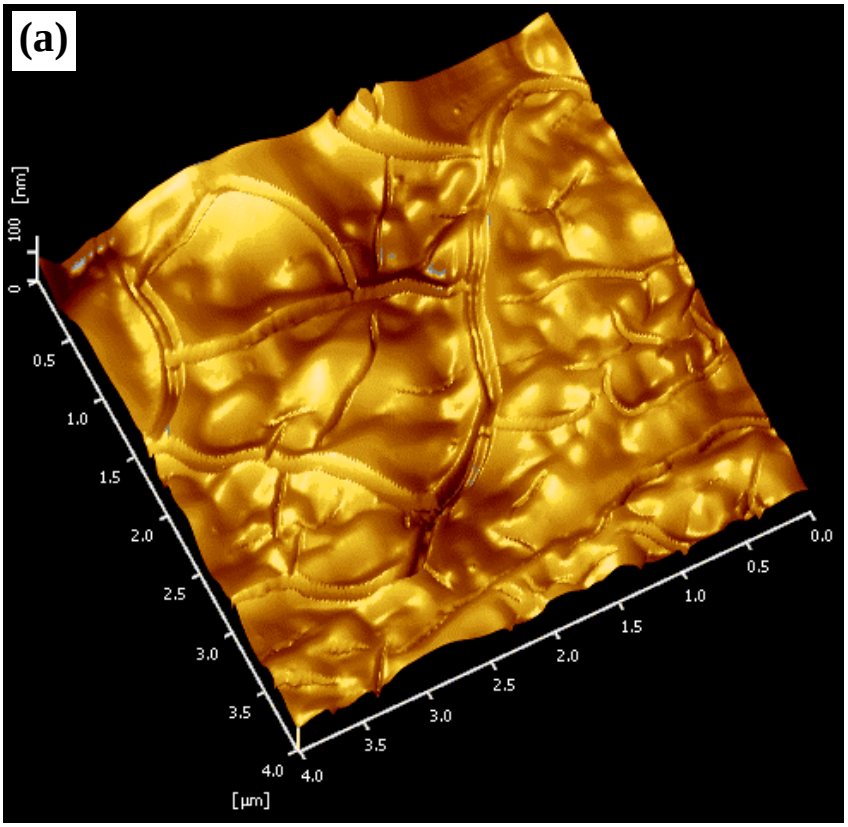

Fig. 3.7a: AFM 3D topological view of stable and unstable grain and subgrain boundaries.

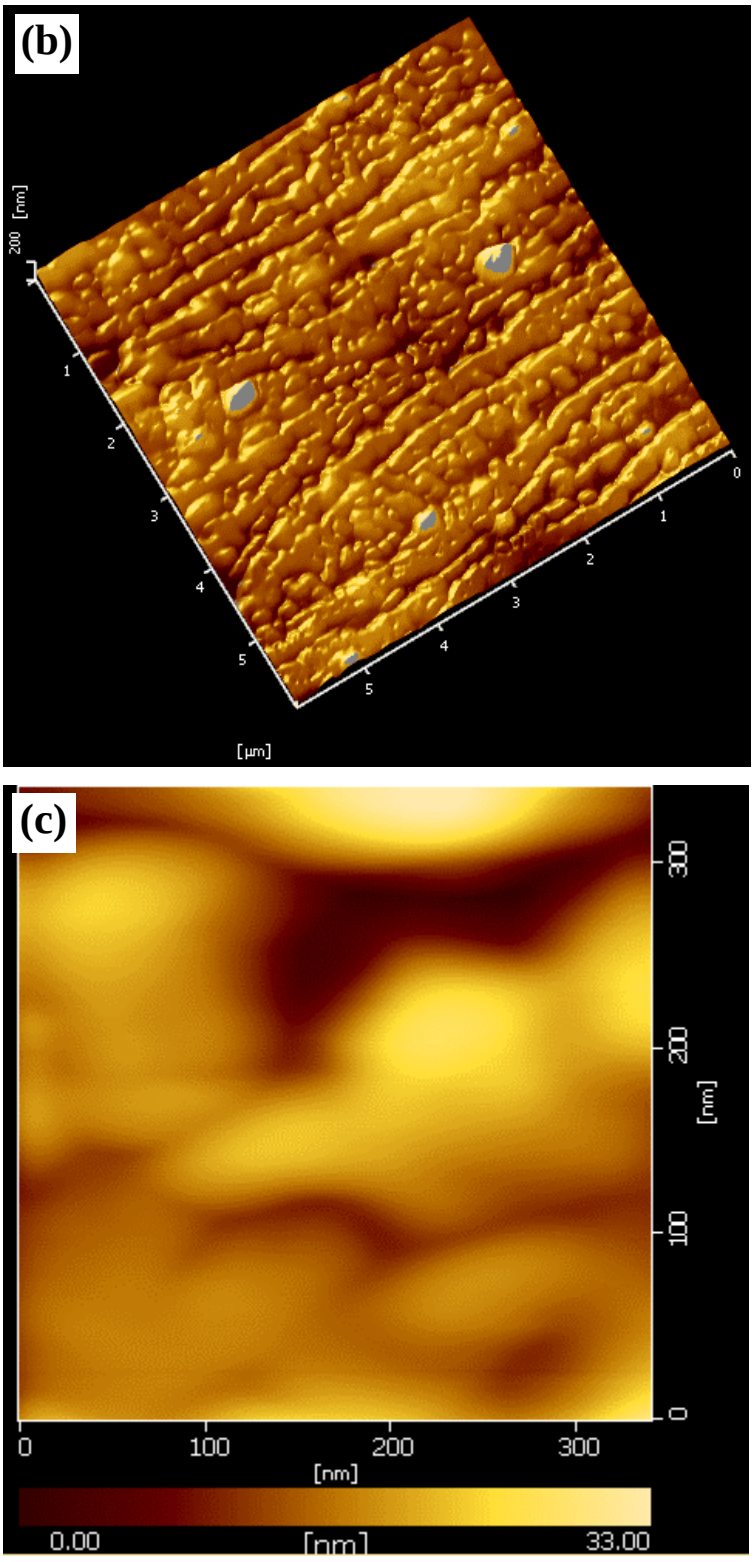

Fig. 3.7 (contd.): AFM totopograph of (b) 5th pass showing equiaxed ultrafine grains aligned in rolling direction (c) 7th pass showing well developed grains of 177 nm.

3.3.2 Tensile properties

The tensile properties have been evaluated for the samples from 0^{th} to 5^{th} pass ARBed materials. Two samples from each pass were tested. The results showed reproducible data for both the samples. All the tests were carried out at room temperature. The results of tensile tests are shown in figure 3.9a & b showing engineering stress-strain as well as true stress-strain diagrams, respectively. The major increase in strength is observed after the first cycle of ARB. However, the relative increment in strength after further ARB passes decreases and no difference was observed between 4^{th} and 5^{th} pass ARBed materials. The characteristic nature of these plots show that the ultimate tensile strength (UTS) and yield strength increases by 116% and 200% respectively after 5^{th} pass of ARB cycle. As the grain size decreases to an ultrafine scale, the strain hardening rate decreases leading to a plunging tensile test curve . The necking starts soon after yielding. This behaviour is also observed in the present tensile tests. The variation in strength and elongation with the number of passes is shown in figure 3.10 for both the samples tested for tensile strength. The values of the strength as well as elongation for both the samples (sample-1 and sample-2) were close to each other indicating reproducibility of the results with respect to the materials homogeneity. The plot shows that elongation for the initial material varies between 31-34% compared to 4-6% in the case of ARBed materials. It is therefore concluded that material strength increases with the lost of ductility during ARB process. The decrease in elongation is very large after 1^{st} pass ARB, however, there is not much difference in elongation with further ARB steps. This indicates a pronounced loss of formability during ARB. The details of these results have been discussed in chapter 4.

3.3.3 Tensile fracture behaviour

For further analysis of the bonding condition in tension and the mode of fracture, the fracture surfaces of the as-ARBed samples after tensile tests are observed under the scanning electron microscopy. The fracture surfaces are shown in figure 3.11. Figure 3.11a shows large size of dimples, with large voids, generated from the initial material.

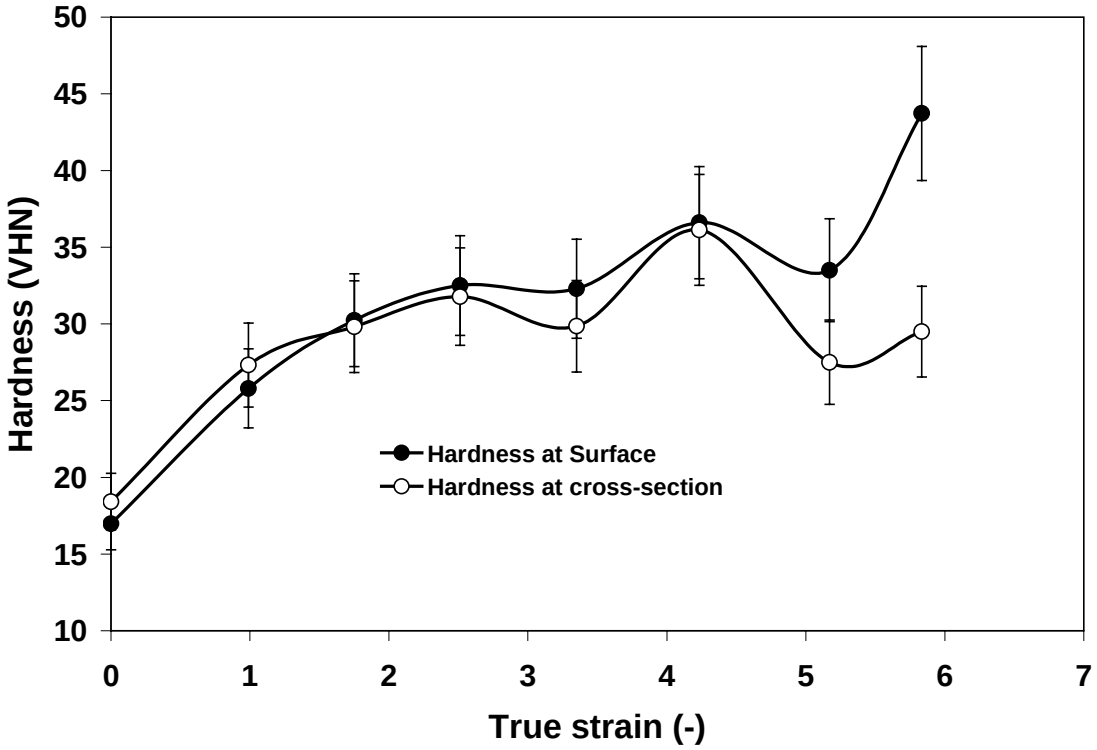

Fig. 3.8: Plot showing hardness variation at surface and the longitudinal cross-section of ARBed samples

This suggests a highly ductile mode of fracture behaviour, which is expected from the composition of the material. Figure 3.11b shows the fractograph of the 1st pass material, showing two distinct layers with debonding at the interface. It seems from the fractograph that the debonding takes place at the interface and, thereafter, individual layers neck and fracture in ductile mode. However, it was observed that the dimple size was smaller than that observed in the initial material. The photograph clearly shows the shear zones on the debonded interfaces. It seems that the bonding quality varies spatially, which is clear from the fact that at some points debonding does not take place. Figure 3.11c shows the fractograph of 2nd pass sample showing debonding at the interfaces as well as breaking of oxide particles. It is obvious from the figure that bonding is basically absent where oxide particle are present. In the outer two layers, it is readily visible that the two layers do not detach, indicating improvement of the interface after the 2nd pass. This fact has also been described in the section 3.1.

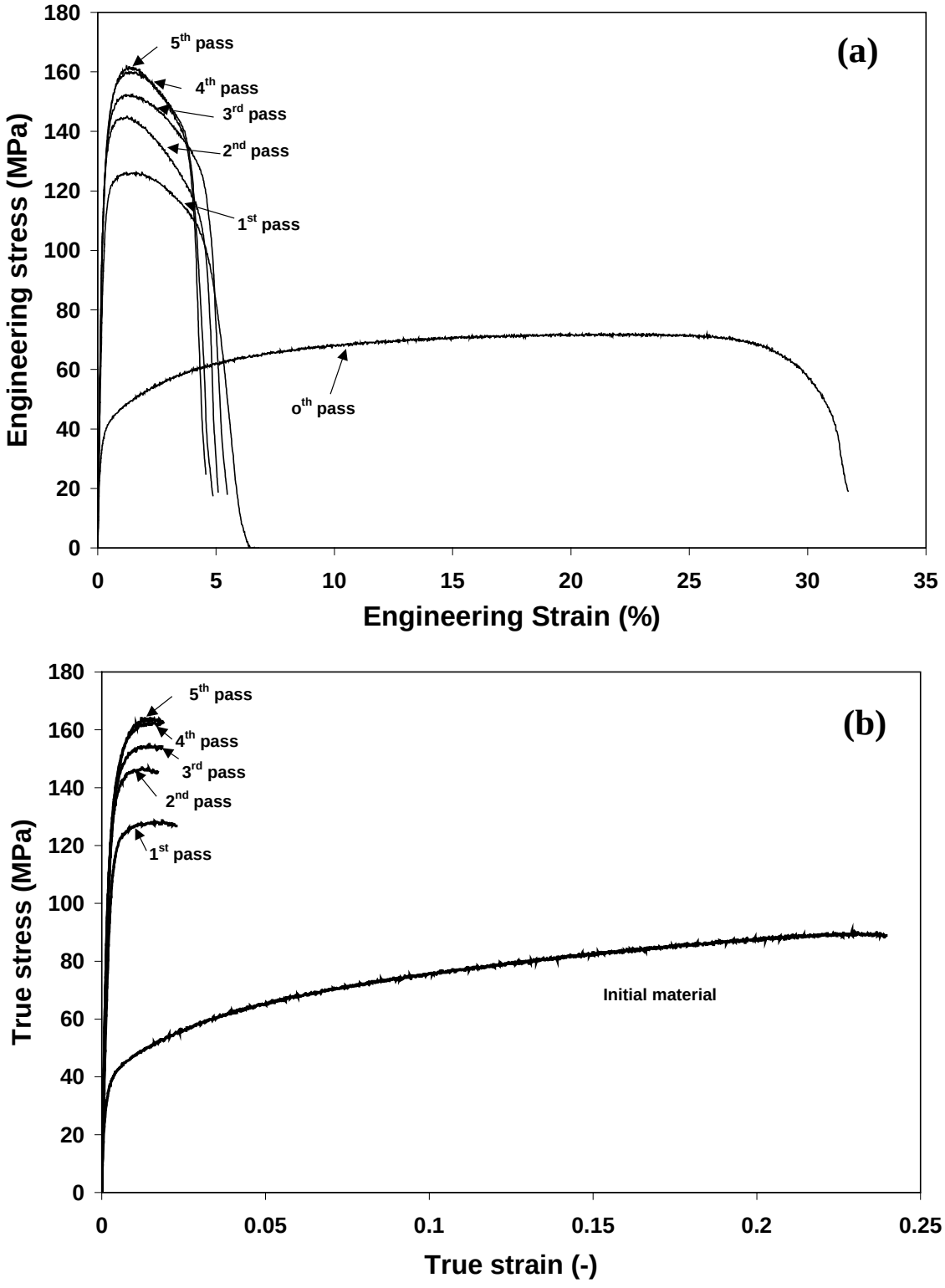

Fig. 3.9: Plots showing (a) engineering stress-strain and (b) true stress-strain curves.

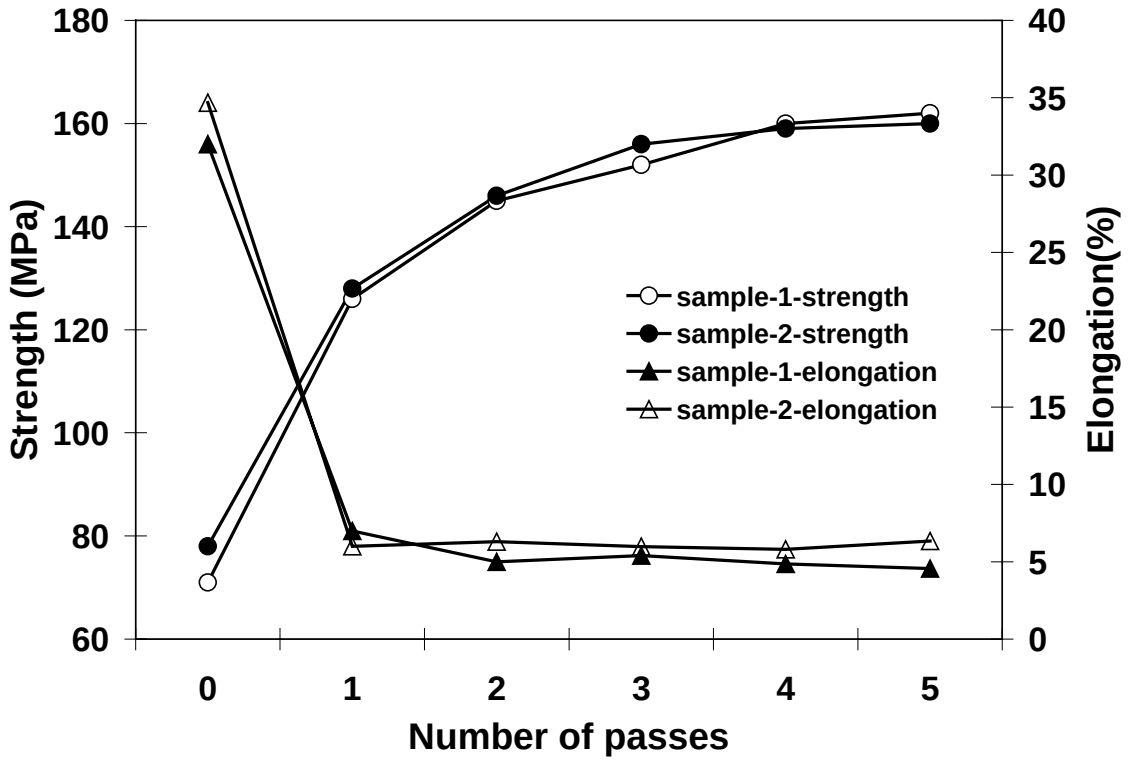

Fig. 3.10: Plot showing variation of strength and elongation with number of ARB passes.

Figure 3.11d shows the fracture surface after 2nd pass, indicating that the dimple size is much smaller compared to that observed in the initial material. This is indicative of the decrease in ductility and creation of large number of voids before necking. Figure 3.11e shows that the portion of debonded interface is highly strained away from a strongly bonded area. This suggests that the bonding between surface does not take place uniformly in terms of bond strength. The broken oxide particles are also seen in the vicinity indicating debonding in that area of interface. It is therefore concluded that the bond strength and the cleanliness of the surfaces before joining may play an important role in determining the final strength of ARBed materials. Figure 3.11f show the fractograph of 4th pass samples, clearly indicating the improvement in bond strength brought forward from the previous passes. Large voids are created during tensile loading where oxide particle existed at the interfaces. Finally, it is clear from the above results

that oxide particle inhibit the bonding and this is reflected in the mechanical properties, when compared to other studies.

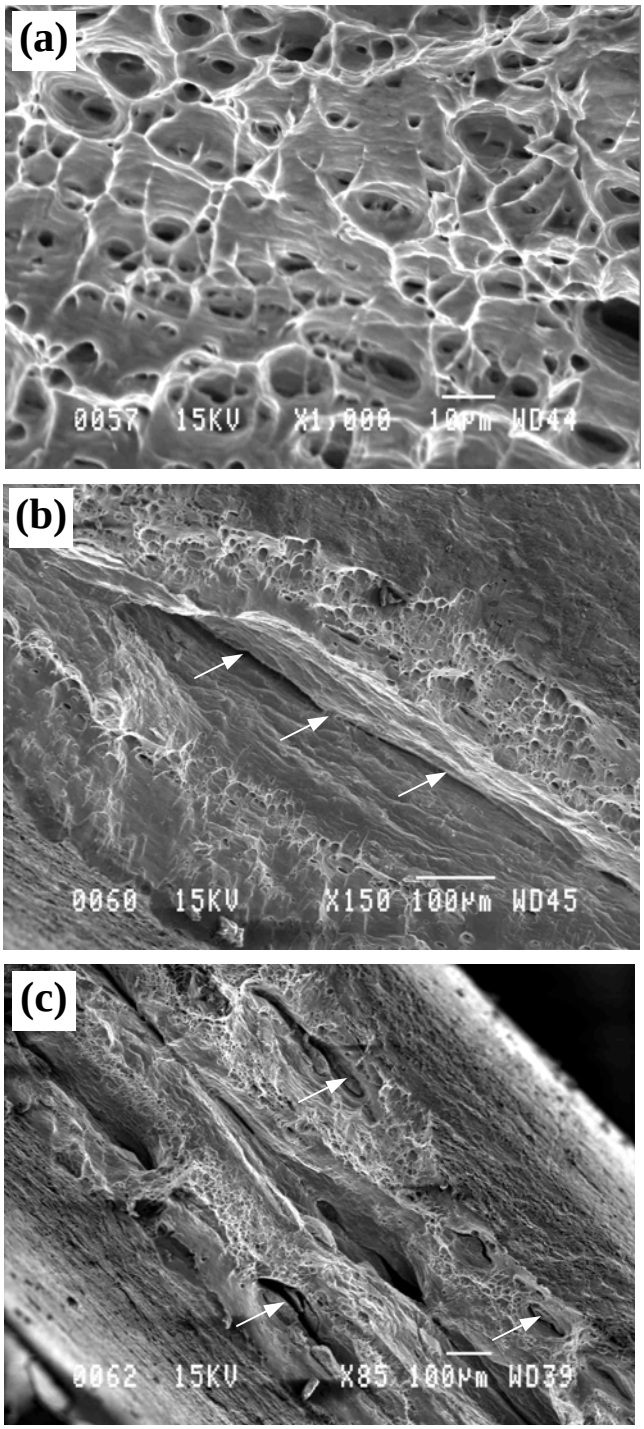

Fig. 3.11: SEM fractographs showing (a) large size dimples in initial materials (b) interface debonding during tensile loading for 1st pass (c) voids at oxide existing sites.

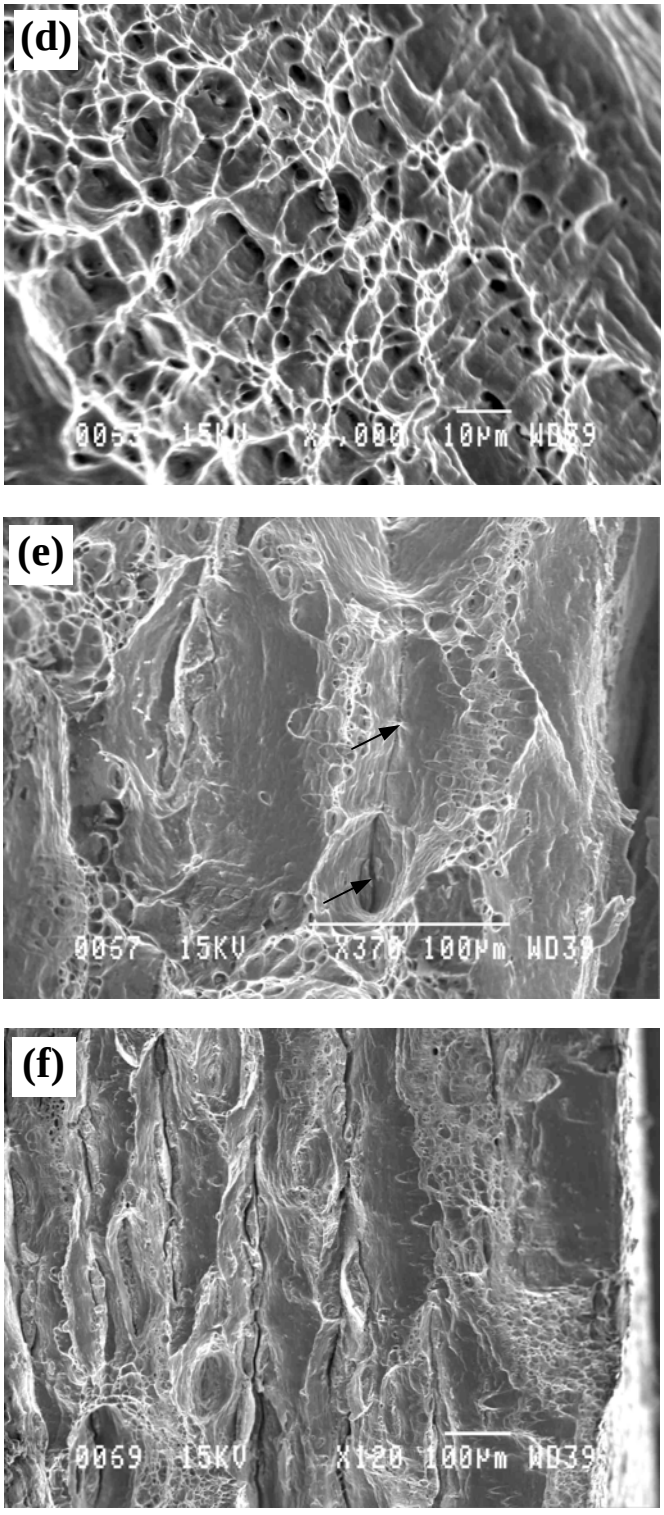

Fig. 3.11 (contd.): SEM fractographs showing (d) smaller dimples in 4th pass (e) strained interface bonds and oxide breaking (f) properly bonded interfaces of previous passes.

3.4 Evolution of Texture

Texture measurement was carried out on the sample after 50% cold rolling. Texture was measured on the mid-plane section. The corresponding {111} pole figure has been presented in Fig.3.12.

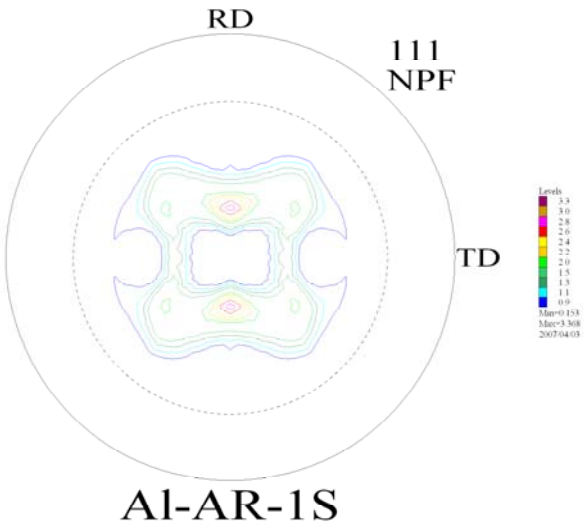

Fig.3.12. Experimental {111} pole figure from mid-plane of 1st pass.

The texture components at this stage are mainly Brass {011}<112> and Cube {001}<100> components. Increasing number of passes show evolution of new texture components as well as diminution of exiting components. The overall texture intensity has been found to vary with increasing number of passes. Fig.3.13 shows the {111} pole figures for 2nd pass to 7th pass of ARBed material. After 2nd pass (fig. 3.13a), the surface texture shows presence of Cu component {112}<111> and S component {123}<634>; at the mid-plane section the brass is the major texture component apart from mild Cu and S components. The texture intensity at the surface is similar to that of the mid-plane. {111} pole figure for 3rd pass (fig. 3.13b)shows Brass, Cu and S component at both the sections; only at the surface there is a slight indication of Cube-ND component. The intensity at the surface is quite higher than the mid-plane section. After 4th pass (fig. 3.13c), there is a complete change in the texture components at the surface; it is basically Cube-ND component. At the mid-plane it is nearly same as that of at the mid-plane section after 3rd pass.

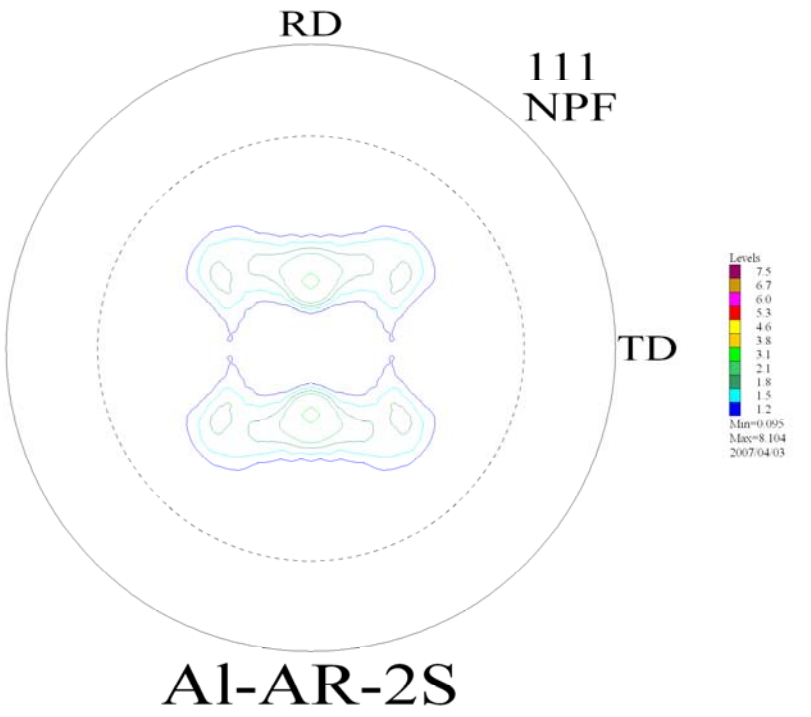

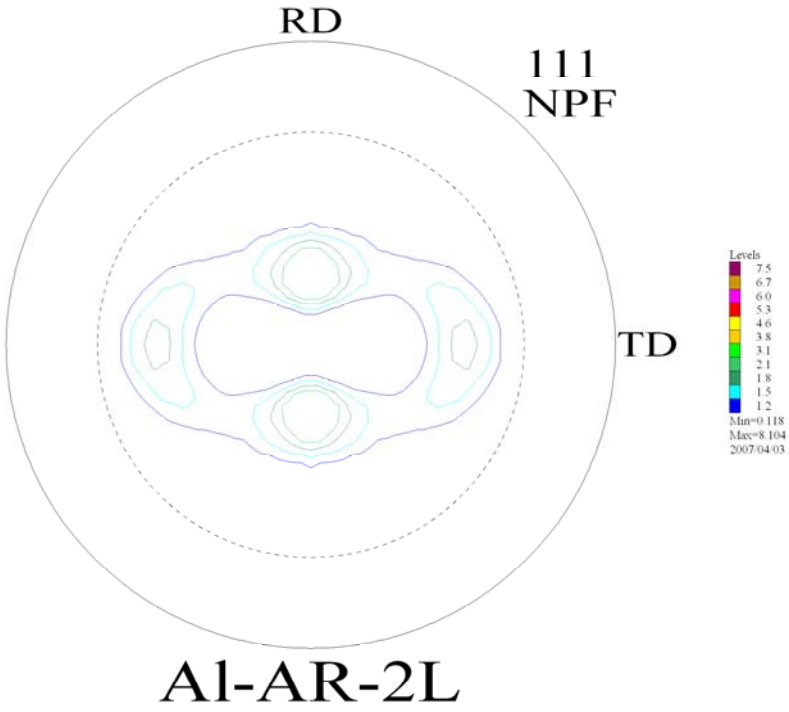

Fig.3.13a: Experimental {111} pole figure from mid-plane (top) and from surface (bottom) of 2nd pass.

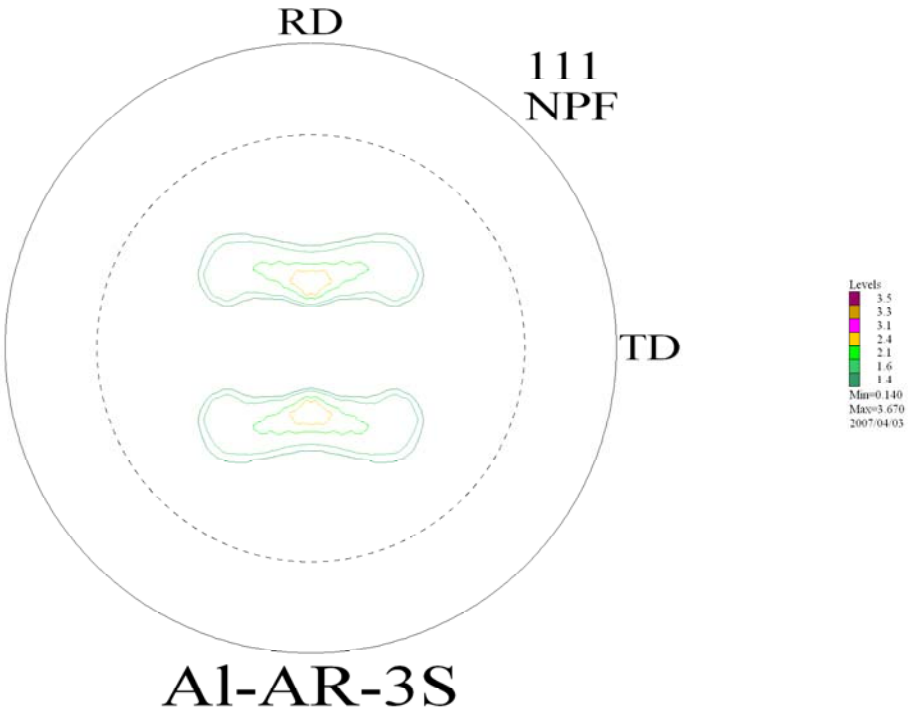

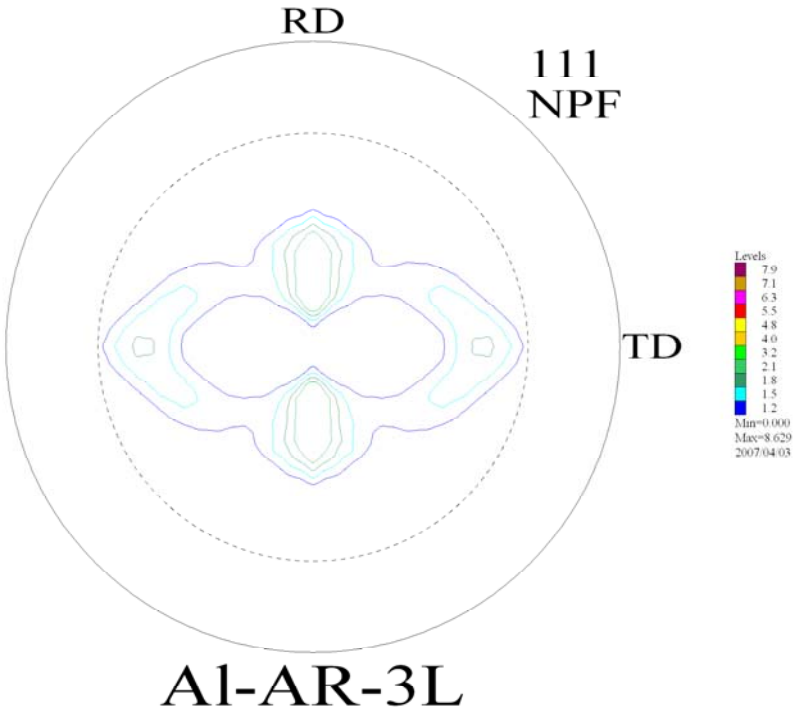

Fig.3.13b: Experimental {111} pole figure from mid-plane (top) and from surface (bottom) of 3rd pass.

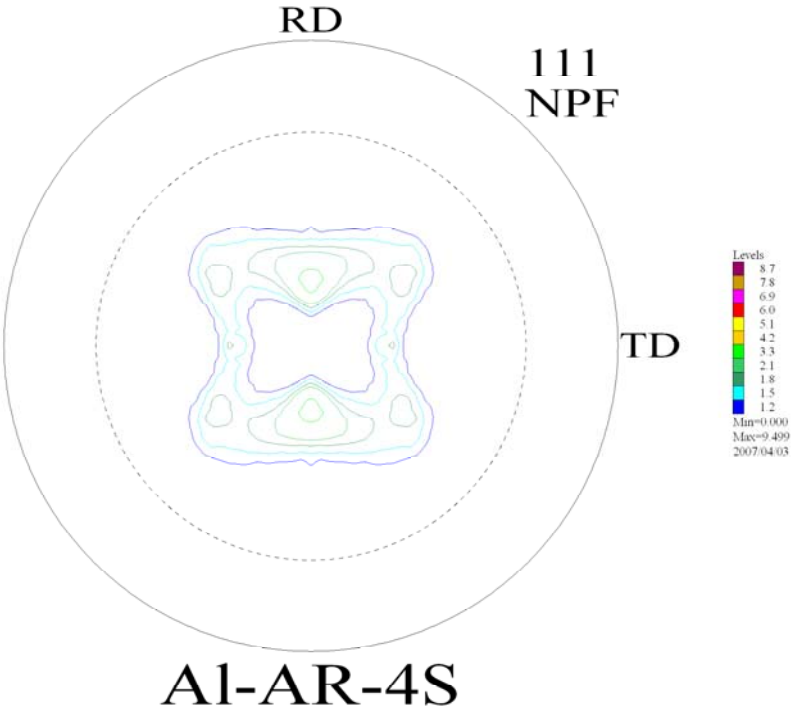

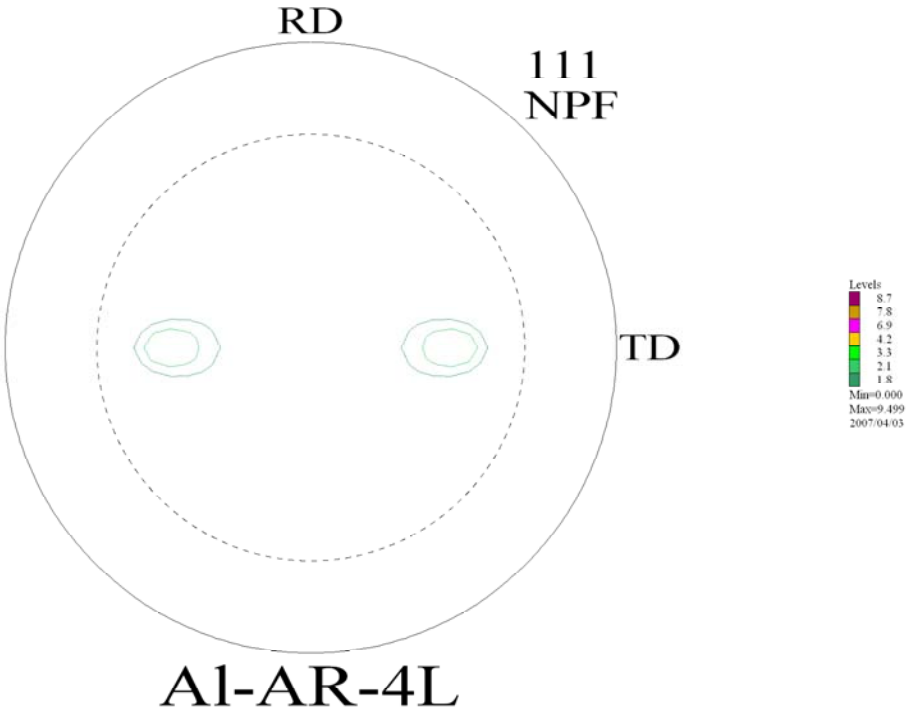

Fig. 3.13c: Experimental {111} pole figure from mid-plane (top) and from surface (bottom) of 4^{th} pass.

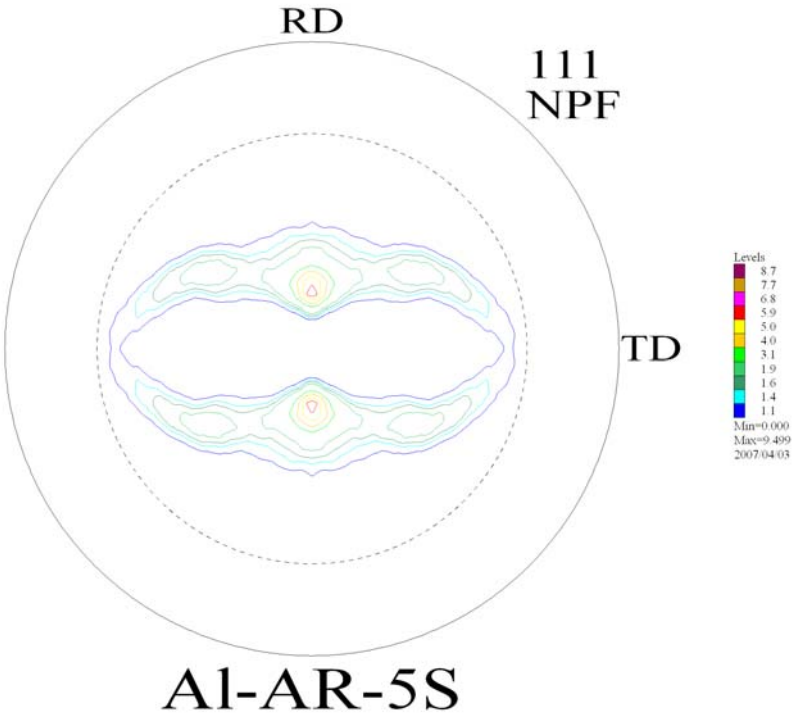

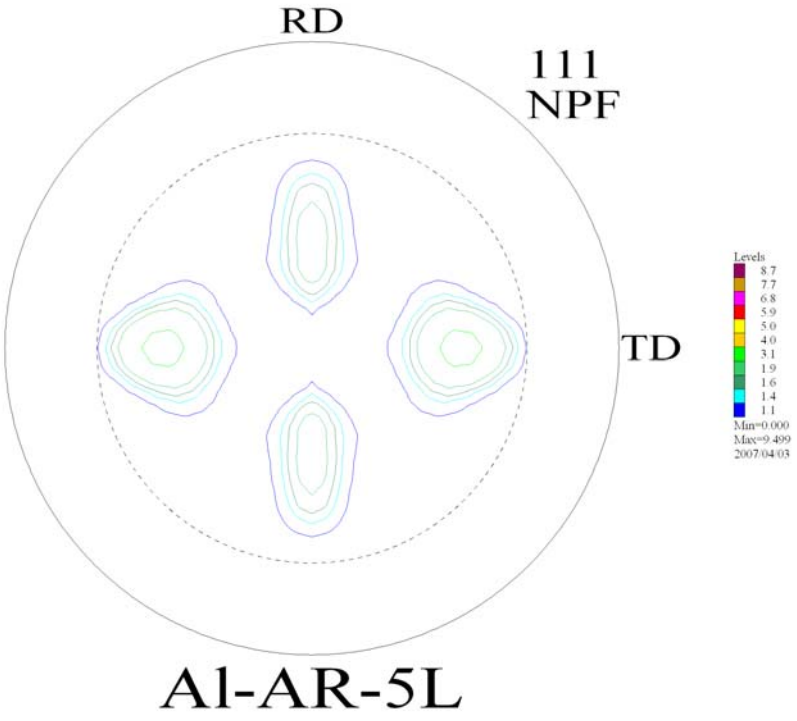

Fig.3.13d: Experimental {111} pole figures from mid-plane (top) and surface (bottom) of 5^{th} pass.

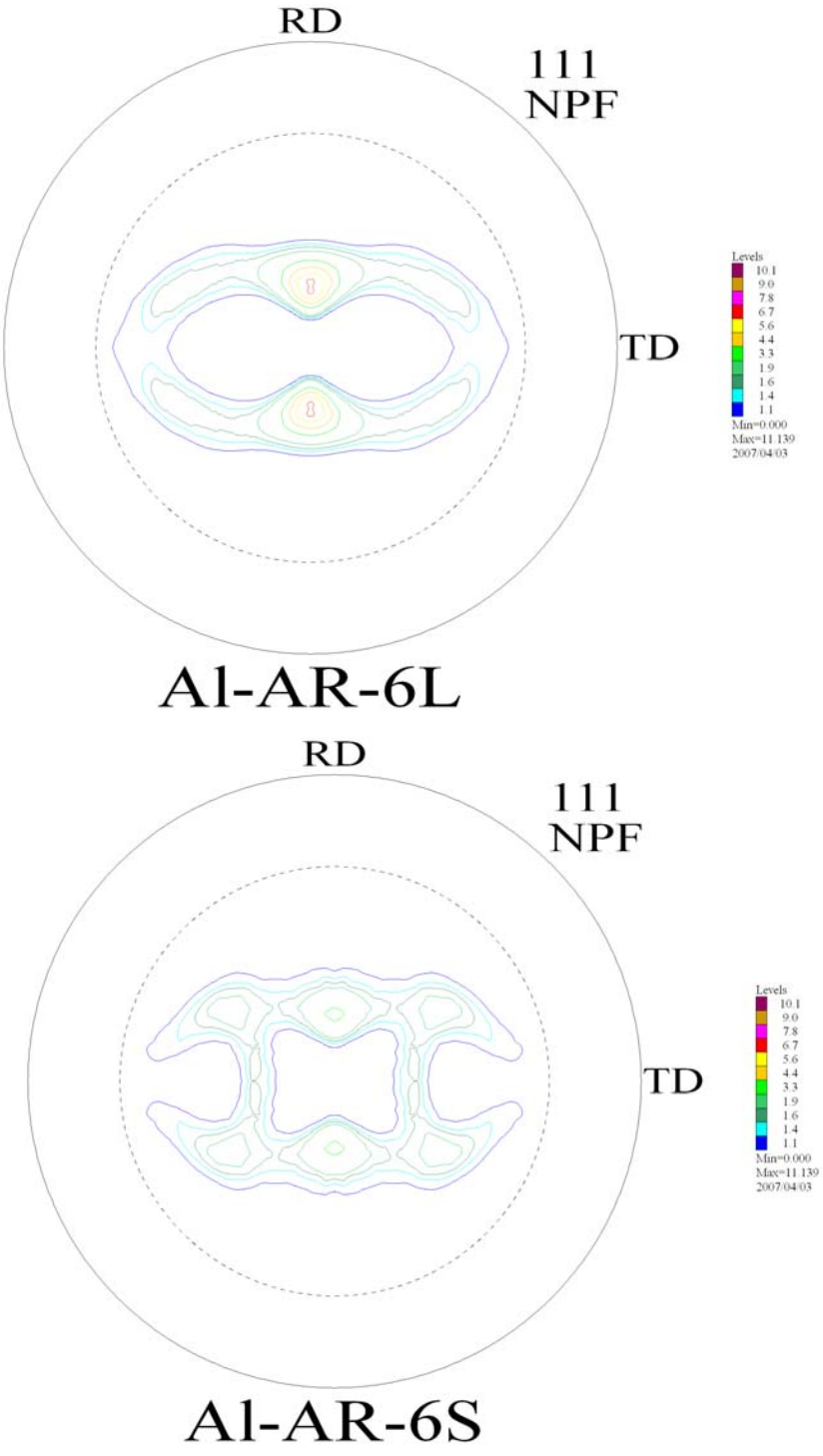

Fig.3.13e: Experimental {111} pole figures from mid-plane (top) and surface (bottom) of 6^{th} pass.

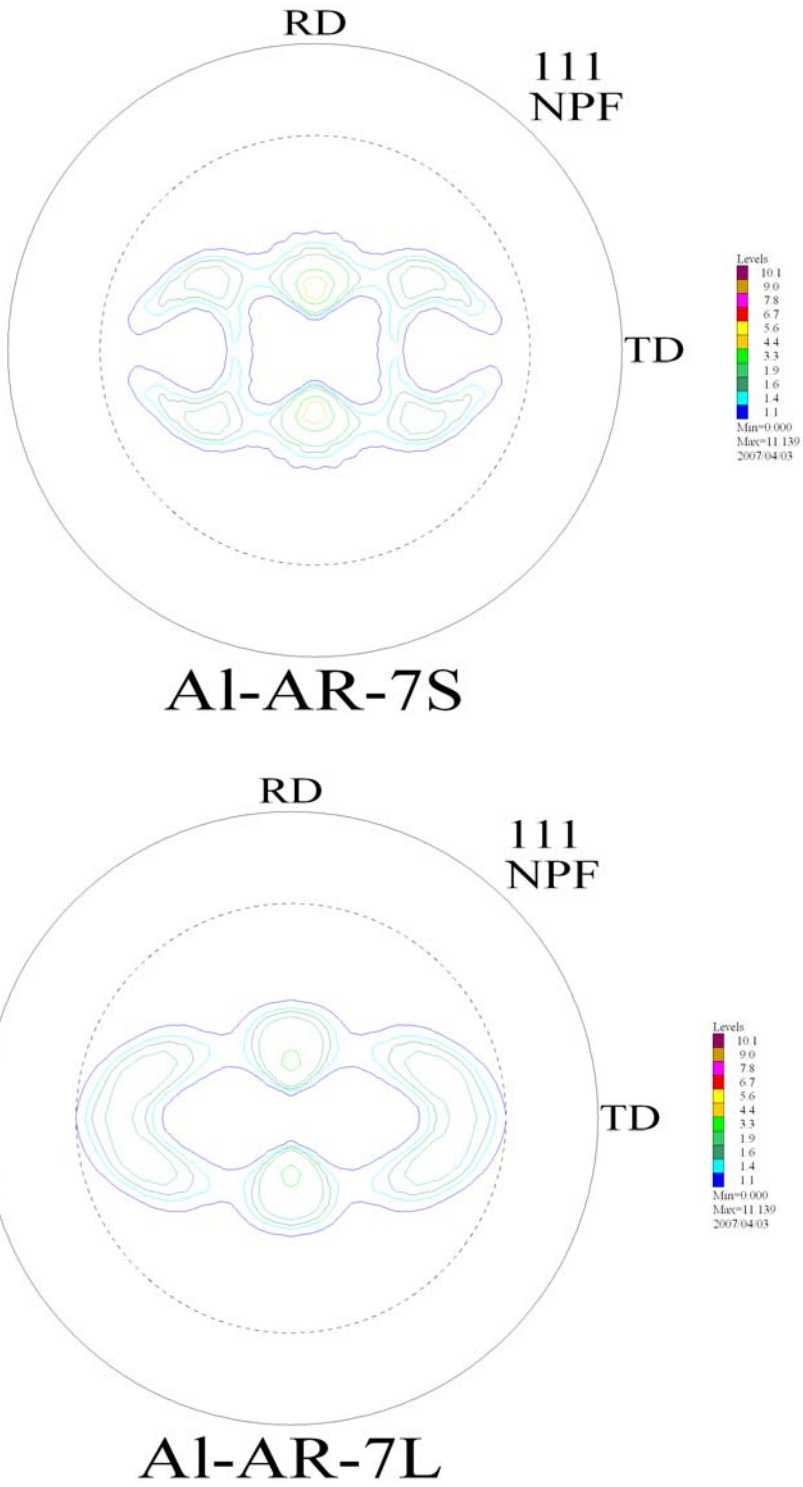

Fig.3.13f: Experimental pole figure of 7th pass from mid-plane (top) and from surface (bottom) of 7th pass.

After 5^{th} pass (fig. 3.13d), the surface showing Cube-ND, nearly similar to that of after 4^{th} pass; but the mid-plane shows presence of Brass, Cu and S components. At this stage there is quite increase in the overall texture intensity. After 6^{th} pass (fig. 3.13e) and 7^{th} pass (fig. 3.13f), there is not much change in the texture components with increasing number of passes as well as in the intensity also. The texture components are also of similar nature i.e. Brass, Cu and S components.

****

CHAPTER-IV

Discussion

Recently, severe plastic deformation (SPD) processing has received considerable attentions for the synthesis of ultrafine grained materials or nanocrystalline materials. The major endeavour of materials scientists has been directed in the development of ultrafine grained materials basically due to the promise of such materials in achieving higher strength to weight ratio and improved physical properties. The top down approach of materials synthesis has given way to SPD in the development of ultrafine grained materials. There are several route to incorporate severe plastic deformation in materials and accumulative roll bonding technique is one of the variants of it. In the present study accumulative roll bonding process has been employed to process commercial purity 1100 Al. Accumulative roll bonding up to seven passes could be done in this study followed by their microstructural analysis and mechanical property evaluation. The result obtained thereof is discussed in light of process conditions and microstructural characteristics.

The results presented in the previous chapter clearly showed that UFG aluminium with sufficient strength could be readily obtained by accumulative roll bonding process. It is practically very important because rolling is the most appropriate process to produce the bulk materials. If this process is applied to practical use, we could obtain high strength. Even pure materials, without any alloying element addition, can be processed by this route to achieve better performance. The complicated thermomechanical treatments associated with conventional alloys can be easily obviated. This process can also address the recent social demands of recycling of materials. The process of ARB is also important from the practicability point of view. Other processes such as ECAP and HPT require sophisticated instruments for processing. On the other hand, rolling technique is one of the most popular ways of plastic working, and the detailed deformation analysis could be easily carried out on materials, compared to that obtained from other variants of SPD.

Although the grain refinement by large straining processes has been paid much attention to, the formation mechanism of the sub-micron size grains has not yet been clarified to a satisfactory level. The detailed study using ARB, now in progress, will

throw some light on the possible mechanisms of microstructural evolution during SPD. The present study shwoed that the initial material strength of 70 MPa sufficiently increases with the number of ARB cycles i.e. strain, and achieves a maximum value of 162 MPa after 5^{th} cycles of ARB and at a strain of 4.23. The hardness of the material also increases from 17 VHN to 43 VHN after 7^{th} cycle of ARB and at true strain of 5.83. The strengthening mechanism of the ARBed material of different passes are very well interrelated with the changes in microstructure observed after corresponding cycles of ARB. The strengthening of the materials up to 5^{th} cycles is mainly due to work hardening, since most of the materials showed conventional subgrain structures with small misorientations and high dislocation densities. The strength is a function of applied strain up to 5^{th} cycle, which is directly related to the internal stress field created during the straining process. In this study, it is found that the grain size decreases after each cycle of the ARB i.e. strain. The effect of grain size on the material yield stress generally followed the empirical Hall-Petch equation: yield stress is inversely proportional to the root square of grain size for large grain sizes. The TEM micrographs of the material up to 5^{th} pass generally shows the subgrains structure with high dislocation density. The abundance of dislocation networks at the grain boundaries and within the grains of the ARBed metals of 1^{st} to 5^{th} cycles of ARB provides obstacles to the movement of the free dislocations in form of tightly packed sessile locks and complex intersection networks of jogs (also called ledges) and sinks during plastic deformation, which in general, lead to enhanced strength and hardness of the materials. Thus, from 1^{st} to 5^{th} cycles of straining, the strain hardening results from mutual obstruction of dislocation glide and intersection. The interaction of dislocations, sessile locks, and the interpenetration of one slip system by another can leave dislocation jogs (ledges) behind. This theory of hardening due to jogs (or forest of sessile dioslocations) was mentioned by Dieter (1986). The work hardenning becomes more pronounced at the large grains because large grains have enough space for significant numbers of dislocation intersections during deformation, while in the smaller grains, dislocation deposit on opposite boundaries directly and result in minimal hardening. This is due to the fact that smaller grain allow less time and less volume for dislocation interaction. An analytical method for polycrystals with different work hardening rates in different grain size samples was proposed by Thomson et al.

(1973) and successfully fit on the experimental results of the current work of severe plastic deformation of the commercially pure aluminium alloy. The model was based on Ashby's idea about separating "statistically stored dislocations" accumulated during deformation and "geometrically necessary dislocations" generated in order to maintain continuty of the polycrystals. It indicates that work hardening rates should be higher in larger grain sizes consistent with the current study. The basic description of this model is that the hardness and strain near the boundary are different than in the grain centers. Away from the boundary, dislocation population is dominated by statistically stored dislocations, while in the boundary regions, different behavior is expected because grain boundaries can act as dislocation sources and sinks. Moreover, high stress field is also present near the grain boundaries. This should affect the local structure. For the larger grain sizes, the statistically stored dislocation term is more important and has great contribution to the yield stress, since the matrix stress is less than the boundary stresses at small strains. These hardening differences arise from differences in statistical and geometrical volume fractions as a function of grain size. A similar explanation of grain size effects on strength due to varying work hardening between grain interiors and near bounderies was used by Gray et al. (1999). However, work hardening behavior is considered to depend on several factors, including deformation temperature, strain rate, grain size, and texture. The texture of the as-ARBed specimen is shown in figure. The influence of texture on work hardening, therefore, can be excluded as the principal controlling variable.

In the present work, the hardness and the strength of the material achieved is less than that achieved by other researchers by accumulative roll bonding of the same material at room temperature (see Table 1.1 of chapter I). This difference in hardness and strength of the material processed by same technique and at the same temperatrue is basically due to the oxide entrapment during roll bonding. The presence of oxide particles on the interfaces of the material after ARB is confirmed on characterising the dislocation etched ARBed samples by scanning electron microscopy to get the idea of the interface and fracture morphology after tensile testing. The SEM micrographs of 1^{st} to 4^{th} cycles of ARB is sufficient to tell the story of effect of oxide particles on the hardness and strength of the ARBed material. The oxide particles create serious debonding as well breakage.

The interface between layers become discontinuous leading to inferior bonding. The discontinuous (non-uniform) presence of oxide particles seized the resistance capacity of the material against the applied stress. As a result, the material fails before the expected value of applied load. If experiments were carried out with some precaution to avoid the oxide entrapment then the expected value of strength could be achieved comparable to other studies. It can be also concluded from the cross-sectional hardness graph of the material that hardness of the material is badly affected due to presence of oxide particles at the interfaces. As the number of interfaces increases from 1^{st} to 7^{th} cycles, the content of oxide particles also increases. This leads to unexpected low hardness values even after large true strains are achieved in subsequent passes. The decrease in the hardness of the material after 6^{th} cycle may be due to the dynamic recovery of the material. The activation energy for atomic diffusion decreases after a certain amount of incorporated strain. This results in easy restoration by dislocation climb and cross-slips.

On the other hand, the evolution of the ultrafine grained structure must contribute to the large strength after 5^{th} cycles. However, the strength may saturated after 5^{th} cycle at which the whole volume in the sheet was filled with the ultrafine grains. The strengthening in the transition region of micrograins to ultrafine grains between 5^{th} to 7^{th} can be also explained by the increase in the volume fraction of the ultrafine grained polycrystals. However, it has been ensured that the UFG polycrystals show the same deformation mechanism as that in conventional materials, which can be explained by dislocation theory.

The texture evolution during ARB showed that there are formation of brass, copper and S component at varying intensity both at the surface and at the mid-plane sections. This continued up to 3^{rd} pass. After 4^{th} pass, although the mid-plane section remains same, the surface texture changes to cube-ND component. This indicates that at this stage there is some changes in strain path at the surface. Presence of cube-ND was observed after 5^{th} pass at mid-section also. Subsequent passes show that again from cube-ND, there is formation of brass, copper and S components after 6^{th} and 7^{th} pass. There was not much change in the textural intensity after 5^{th} pass onwards.

Therefore, the texture evolution in this material shows formation of brass, copper and S components after 7^{th} pass. It passes through a transition after 4^{th} pass, which might be due to additional strain component arising on the surface.

****

Conclusions

The present work on the accumulative roll bonding of commercial purity Al showed some interesting results in terms of microsctructural characteristics and the mechanical properties, which is presented in chapter III. These results have been discussed in detail in chapter IV. In view of these, the following conclusions could be drawn from this study.

- Accumulative roll bonding of commercially pure Al sheets could be done to achieve at true strain of 5.83.
- The process was limited by the occurrence of cracking of the edges, caused by the state of stress at that location and improper cutting of the sheets before rolling.
- The yield stress increases with increasing strain and decreasing grain size of the experimental material. However, the ductility decreases to very low levels.
- The hardness value doubled after 4 passes of ARB.
- The most pronounced change in the mechanical properties and the microstructural features were observed to occur after the first cycle of ARB
- Ultrafine grains, having a mean grain size in the range 1 μm, was successfully produced.
- The ultrafine grains partially formed after 3^{rd} cycle of ARB, and after 7^{th} cycle, the materials showed ultra-fine grains of mean size 500-800nm.
- The change in mechanical properties corresponding with the change in microstructure related very well
- The texture evolution shows formation of brass, copper and S components both at the mid-plane as well as at the surface.

****

Scope for future work

In the course of experimentation, certain observations are made in order to achieve the desired objectives successfully. Due to the paucity of time, these could not be attempted in the present investigation. Therefore, an attempt has been made in this section to elaborate on the future possibilities in this area and remedies, which could be taken care of in any future endeavours.

- The data of tensile testing of the specimens of 6^{th} and 7^{th} cycle of ARB are very important to optimize the trends of strength and ductility and effects of oxide particles on the material after corresponding cycle of ARB.
- The variation in hardness of the material should be taken by micro- or nano-indentation to avoid the influence of imperfection.
- For tensile testing, very small size tensile samples should be used to avoid influence of voids that might adversely influence the mechanical response of the material.
- The SAD pattern should be taken from the regions having diameters of 3µm that gives the simple pattern either scattered or single net pattern.
- During the accumulative roll bonding process of the experimental material, the cracks at the edges of the ARBed material should be trimmed to avoid further crack propagation.

As already mentioned, when a coarse grained material is severely deformed to transformed it into ultrafine grained/nanocrystalline materials by severe plastic deformation methods, the physical and mechanical properties of the material completely changed. Among these properties the most interesting are the changes in Curie and Debye temperatures, diffusion and thermal coefficients. Another example is the change in elastic properties of the material. These changes greatly influence the thermal, optical, magnetic, electrical and mechanical properties of the materials. Therefore these changes open the

door of new research for future researchers. By estimating the changes in physical and mechanical properties of the material after ARB process, one can decide on the suitable practical applications of ARBed materials. From the practical point of view, it is important to acknowledge that recent studies have demonstrated very clearly a great potential for the use of SPD processing and the incorporation of ARB in industrial applications. There are very good reasons for believing that, in the relatively near future, SPD processing will become established as the basis for the commercial production of semi-products and products with UFG structures using a wide range of metals and alloys.

****

REFERENCES

Anderson P M, Bingert A M, Misra A, Hirth J P, Acta Mater, 51 (2003) 6059.

Armstrong R W, Huges D A, Advanced Materials for the Twenty-First Centutry: The Julia Weertman Symposium ed. Y.W. Chung, Warrendale, PA (1999) 409.

Asaro A R , Krysl P, Kad B, Philos.Mag., 83 (2003) 733.

Beygelzimer Y, Varyukhin V, Orlov D, Synkov S, Spuskanyuk A, Pashinska Y, In: Zehetbauer M J, Valiev R Z, editors. Nanomaterials by severe plastic deformation. Weinheim, Germany: Wiley–VCH Verlag (2004) 511.

Bird J E, Mukherjee A K, Dorn J E, in: D G Brandon, A. Rosen (Eds.) Quantitative Relation between properties and microstructure, Israel (1969) 255.

Chinh N Q, Szommer P, Horita Z, Langdon T G, Adv Mater., 18 (2006) 34.

Chokshi A K, Scripta Mater., 23(1989) 1679.

Chu HS, Liu KS, Yeh JW. Scripta Mater 2001;45:541.

Dieter G E, "Mechanical Metallurgy", 3rd edition, McGraw-Hill Book Company, New York, NY, 1986, pp. 231.

Erb U, El-Sherik AM, Palumbo G, Aust KT, Nanostruct Mater, 2 (1993) 383.

Furukawa M, Horita Z, Langdon TG, Metals Mater, 9 (2003) 141.

Gifkins R C, Langdon T G, J Inst Metals, 93 (1964–65) 347.

Gleiter H, In: Hansen N, Horsewell A, Leffers T, Lilholt H, editors. Deformation of polycrystals: Mechanisms and microstructures. Roskilde, Denmark: Risø National Laboratory; (1981) 15.

Gleiter H, Prog Mater Sci. 33 (1989) 223.

Gray G T, Chen S R, Vecchio K S, Metal. Mater. Trans., 30A (1999) 1235.

Hall E O, Proc Roy Soc B, 64 (1951) 747.

Han B Q, Matejczyk D, Zhou F, Zhang Z, Bampton C, Lavernia E J, Metall Mater Trans, 35A (2004) 947.

Hofmann D C, Vecchio K S, Mater Sci Eng, A402 (2005) 234.

Horita Z, Furukawa M, Nemoto M, Langdon T G, Mater Sci Tech, 16 (2000) 1239.

Huang J Y, Zhu Y T, Jiang H, Lowe TC, Acta Mater, 49 (2001) 1497.

Hughes D A, Hansen N, Acta Mater., 45 (1997) 3871.

Hughes D A, Hansen N, Acta Mater., 48 (2000) 2985.

Koch C C, Sripta Mater., 49 (2003) 657.

Koch CC, Cho YS, Nanostruct Mater, 1(1992) 207.

Krallics G, Lenard J G, J. Mater.Proc.Tech, 152 (2004) 154.

Langdon T G, Acta Metall. Mater, 42 (1994) 2437.

Lapovok R, J. Mater. Sci., 40 (2005) 1.

Lee S H , Saito Y, Tsuji N, Utsunomiya H, Sakai T, Scripta Mater, 46 (2002) 281.

Li B L, Tsuji N, Kamikawa, Mater.Sci. Eng, A423 (2006) 331.

Li J C M, Trans.Met.Soc., 227 (1963) 239.

Liao X Z, Appl. Phys.Lett., 83 (2004) 3564.

Liao X Z, Appl.Phys.Lett., 83 (2003) 5062.

Liu Q, Huang X, Lloyd D J and Hansen N, Acta Mater., 50 (2002) 3789.

Lu L, Science, 304 (2004) 422.

Luton M J, Jayanth C S, Disko M M, Matras S and Vallone J, Mater Res Soc Symp Proc 132 (1989) 79.

Meyers M A, Mishra A, Benson D J, Prog. Mater Sci, (2005) 443.

Mishra R S, Ma ZY, Mater Sci Eng, R50 (2005) 1.

Nabarro F R N, Report of a conference on strength of solids, the physical society, London, UK,1948,P.75 and C. Herring, J. Appli. Phys., 21 (1950) 437.

Nemoto M, Horita Z, Furukawa M, Langdon T G, Metals Mater, 4 (1998) 1181.
Pande C S, Masumura M A and Armstrong R W, Nanostruct. Mater, 2 (1993) 323.

Petch N J, J Iron Steel Inst, 174 (1953) 25.

Rhodes C G, Mahoney M W, Bingel W H, Spurling R A, Bampton C C, Scripta Mater, 36 (1997) 69.

Richert J, Richert M, Aluminium, 62 (1986) 604.

Richert M, Liu Q, Hansen N, Mater Sci Eng, 260A (1999) 275.
Saito Y, Tsuji N, Utsunomiya H, Sakai T and Hong R G, Scripta Mater, 39 (1998) 1221.

Salishchev G A, Valiahmetov O R, Galeev R M, J Mater Sci, 28(1993) 2898.

Segal V M, Reznikov V I, Drobyshevskiy A E, Kopylov V I, Russian Metall, 1 (1981) 99.

Shin D H, Park J J, Kim Y S, Park K T, Mater Sci Eng, A328 (2002) 98.

Sitdikov O, Sakai T, Goloborodko A, Miura H, Kaibyshev R, Mater Trans, 45 (2004) 2232.

Smirnova N A, Levit V I, Pilyugin V I, Kuznetsov R I, Davydova L S, Sazonova VA, Fiz Met Metalloved, 61 (1986) 1170.

Thompson A W, Baskes M I, Flangan W F, Acta Metall., 21 (1973) 1017.

Tsuji N, Saito Y, Lee S H, Minamino H, Adv. Eng. Mater, 5 (2003) 338.

Valiev R Z, Islamgaliev R K, Alexandrov I V, Prog Mater Sci, 45 (2000) 103.

Valiev R Z, Korznikov A V, Mulyukov R R, Mater. Sci. Eng, A168 (1993) 141.

Valiev R Z, Krasilnikov N A, Tsenev N K, Mater Sci Eng, 137A (1991) 35.

Valiev R Z, Mulyukov R R, Ovchinnikov V V, Philos Mag Lett, 62(1990) 253.

Valiev R Z, Nanostruct Mater, 3 (2004) 511.

Valiev R Z, Nature Mater, 3 (2004) 511.

Valieve R Z, Estrin Y, Horita Z, Langdom T G, .Zehetbauer M J, Zhu Y T, JOM April (2006) 33.

Valitov V A, Salishchev G A, Muhtarov H, Russian Metall, 3 (1994) 127.

Varyutkhin V N, Beygelzimer Y Y, Synkov S, Orlov D, Mater Sci Forum, 503-504 (2006) 335.

Vorhauer A, Mater. Sci. Forum, 503-504 (2005) 299.

Wang J T, Mater Sci Forum, 503-504 (2006) 363.

Wang Y, Chen M, Zhou F, Ma E, Nature, 419 (2002) 912.

Witkin D B, Lavernia E J, Prog Mater Sci, 51(2006) 1.

Xu C, J. Mater. Eng. Perform., 13 (2004) 683.

Zehetbauer M, Acta Mat., 47 (1999) 1053.

Zhao X, Jing T F, Gao Y W, Zhou J F, Wang W, Mater Lett, 58 (2004) 2335.

Zhilyaev A P, Nurislamova G V, Kim B K, Baro M D, Szpunar J A, Langdon TG, Acta Mater, 51 (2003) 753.

Zhu Y T, Liao X Z, Nature Materials, 39 (2004) 351.

Zhu Y T, Jiang H, Huang J, Lowe TC, Metall Mater Trans, 32A (2001) 1559.

****